Extended Rodlike Polyaromatic Receptors with Bent Tridentate Units Complexed to Lanthanide Metal Ions

Homayoun Nozary,[†] Claude Piguet,*[,†] Jean-Pierre Rivera,[†] Paul Tissot,[†] Gérald Bernardinelli,[‡] Nathalie Vulliermet,[§] Jacques Weber,[§] and Jean-Claude G. Bünzli[||]

Department of Inorganic, Analytical, and Applied Chemistry, Department of Physical Chemistry, and Laboratory for X-ray Crystallography, University of Geneva, CH-1211 Geneva 4, Switzerland, and Institute of Inorganic and Analytical Chemistry, University of Lausanne, CH-1015 Lausanne, Switzerland

Received March 29, 2000

A synthetic strategy is developed to attach semirigid lipophilic sidearms to the 6-positions of bent aromatic tridentate 2,6-bis(benzimidazol-2-yl)pyridine cores to produce U-shaped ligands, $L^{6,7}$. Differential scanning calorimetry (DSC) reveals that entropic contributions severely affect the isotropization processes of these flexible receptors, but no mesomorphism is detected. The attachment of oxygen linkers to the 5- or 6-positions of the benzimidazole sidearms lowers the ligand-centered $^1\pi\pi^*$ and $^3\pi\pi^*$ excited states, and the semiempirical ZINDO method assigns this effect to a destabilization of the HOMO orbitals resulting from π-interactions. Reactions of L^6 with $Ln(NO_3)_3 \cdot xH_2O$ provide the rodlike 1:1 complexes $[Ln(L^6)(NO_3)_3]$ (Ln = La−Lu), which are stable in the solid state but partially dissociate in acetonitrile. The crystal structure of $[Lu(L^6)(NO_3)_3]\cdot CH_3CN$ (**18a**, $LuC_{63}H_{84}N_9O_{13}$, monoclinic, $P2_1/n$, $Z = 4$) reveals an I-shaped arrangement of the ligand strand arising from the meridional complexation of the bent tridentate unit to nine-coordinate Lu(III). The replacement of nitrate anions with trifluoroacetate anions gives the centrosymmetric dimer $[Lu(L^6)(CF_3CO_2)_3]_2$ (**23**, $Lu_2C_{134}H_{162}N_{10}O_{20}F_{18}$, triclinic, $P\bar{1}$, $Z = 1$), in which the symmetry-related Lu atoms are connected by two bridging carboxylates, leading to an H-shaped dimetallic edifice. These complexes $[Ln(L^6)(NO_3)_3]$ and $[Ln(L^6)(CF_3CO_2)_3]_2$ fulfill the geometrical criteria required by precursors of calamitic metallomesogens, but no mesomorphism can be detected, while photophysical studies indicate that the low energies of ligand-centered $^3\pi\pi^*$ excited states drastically limit the luminescence of Eu(III) complexes. The relationships between structural and electronic properties resulting from 5- or 6-substitutions of the benzimidazole rings and the effects of these substitutions on photophysical and thermal properties are discussed.

Introduction

Since the recognition that polar achiral bent-core molecules can produce tilted chiral layered smectic C mesophases with ferroelectric properties suitable for fast-switching electrooptical devices,[1] much interest has been focused on the introduction of 1,3-disubstituted phenylene units into extended rodlike architectures.[2] Surprisingly, the inherent curvature associated with semirigid triaromatic units consisting of a central six-membered ring substituted at the 1- and 3-positions by two lateral aromatic rings (as found in 2,2′:6′,2″ terpyridine, L^1 (Chart 1)) has been poorly exploited in this context[3] although the introduction of chelating heterocyclic binding units offers fascinating possibilities for the design of d- and f-block metallomesogens.[4] The complexation of L^1 with lanthanide metal ions, Ln(III), is well-documented,[5] and stable 1:1 complexes $[Ln(L^1)X_3]$ ($X = Cl^-$, Br^-, OAc^-, NO_3^-) can be easily prepared.[6] We have shown that the attachment of five-membered rings to the central pyridine ring in the related extended tridentate ligand 2,6-bis(benzimidazol-2-yl)pyridine, L^2, improves the affinity for Ln(III) ions, leading to the neutral complexes $[Ln(L^2)(NO_3)_3]$, in which the cis-cis bent aromatic core is roughly planar and meridionally tricoordinated to Ln(III).[7] Electronic and optical properties can be modulated by the judicious choice of the substituents $R^{1,2}$, and crystal structures of the resulting complexes suggest that the attachment of semirigid linear lipophilic groups to the 6-positions of the

* Corresponding author. E-mail: Claude.Piguet@chiam.unige.ch.
[†] Department of Inorganic, Analytical, and Applied Chemistry, University of Geneva.
[‡] Laboratory for X-ray Crystallography, University of Geneva.
[§] Department of Physical Chemistry, University of Geneva.
[||] Institute of Inorganic and Analytical Chemistry, University of Lausanne.

(1) Niori, T.; Sekine, T.; Watanabe, J.; Furukawa, T.; Takezoe, H. *J. Mater. Chem.* **1996**, *6*, 1231. Link, D. R.; Natale, G.; Shao, R.; Maclennan, J. E.; Clark, N. A.; Körblova, E.; Walba, D. M. *Science* **1997**, *278*, 1924.
(2) Shen, D.; Pegenau, A.; Diele, S.; Wirth, I.; Tschierske, C. *J. Am. Chem. Soc.* **2000**, *122*, 1593. Shen, D.; Diele, S.; Wirt, I.; Tschierske, C. *Chem. Commun.* **1998**, 2573. Heppke, G.; Moro, D. *Science* **1998**, *279*, 1872.
(3) Neve, F.; Ghedini, M.; Crispini, A. *Chem. Commun.* **1996**, 2463. Neve, F.; Ghedini, M.; Francescangeli, O.; Campagna, S. *Liq. Cryst.* **1998**, *24*, 673.
(4) For reviews on metallomesogens, see: Donnio, B.; Bruce, D. W. *Struct. Bonding* **1999**, *95*, 194. Binnemans, K.; Bruce, D. W.; Collinson, S. R.; Van Deun, R.; Galyametdinov, Y. G.; Martin, F. *Philos. Trans. R. Soc. London, Ser. A* **1999**, *357*, 3063. Binnemans, K. *Mater. Sci. Forum* **1999**, *315*−*317*, 169. *Metallomesogens*: *Syntheses, Properties and Applications*; Serrano, J. L., Ed.; VCH: Weinheim, Germany, 1996. Hudson, S. A.; Maitlis, P. M. *Chem. Rev.* **1993**, *93*, 861. Bruce, D. W. *J. Chem. Soc., Dalton Trans.* **1993**, 2983.
(5) Constable, E. C. *Adv. Inorg. Chem. Radiochem.* **1986**, *30*, 69.
(6) Kepert, C. J.; Wei-Min, L.; Semenova, L. I.; Skelton, B. W.; White, A. H. *Aust. J. Chem.* **1999**, *52*, 481. Semenova, L. I.; White, A. H. *Aust. J. Chem.* **1999**, *52*, 507. Semenova, L. I.; Sobolev, A. N.; Skelton, B. W.; White, A. H. *Aust. J. Chem.* **1999**, *52*, 519 and references therein.
(7) Piguet, C.; Williams, A. F.; Bernardinelli, G.; Moret, E.; Bünzli, J.-C. G. *Helv. Chim. Acta* **1992**, *75*, 1697. Petoud, S.; Bünzli, J.-C. G.; Schenk, K. J.; Piguet, C. *Inorg. Chem.* **1997**, *36*, 1345.

10.1021/ic000338u CCC: $19.00
Published on Web 10/27/2000

Chart 1

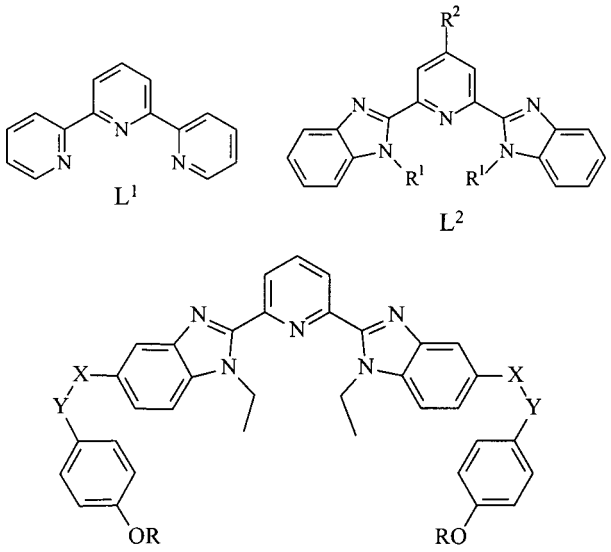

$X = CH_2, Y = O, R = C_{12}H_{25} : L^3$
$X = O, Y = CO, R = C_{12}H_{25} : L^4$
$X = O, Y = CH_2, R = C_{12}H_{25} : L^5$
$X = CH_2, Y = O, R = CH_3 : L^8$
$X = O, Y = CH_2, R = CH_3 : L^9$

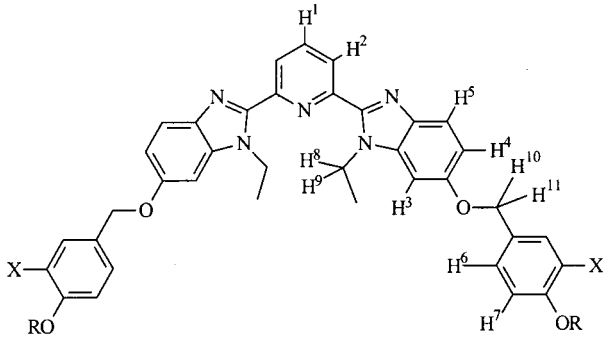

$X = H, R = C_{12}H_{25} : L^6$
$X = OC_{12}H_{25}, R = C_{12}H_{25} : L^7$
$X = H, R = CH_3 : L^{10}$

benzimidazole rings should give rodlike architectures compatible with calamitic mesomorphism.[8] Interestingly, the uncoordinated tridentate unit in L^2 adopts the alternative trans-trans conformation, which corresponds to an interconversion of the 5- and 6-positions of the benzimidazole ring occurring upon complexation to Ln(III) (Figure 1).[7,8] For synthetic reasons, substitution at the 5-position was first performed and ligands L^{3-5} were then synthesized via multistep strategies.[8] Their trans-trans conformation ensures a quasi-linear arrangement of the semirigid lipophilic tails, thus giving rodlike receptors with a rich calamitic mesomorphism (smectic A, smectic C, and nematic) that can be modulated by the nature of the bridging groups (X) between the bent core and the lateral chains.[8] A detailed investigation of the 1:1 complexes $[Ln(L^3)(NO_3)_3]$ (Ln = La−Lu) confirms the formation of U-shaped architectures (cis-cis conformation of the tridentate unit), and we tentatively attribute the resulting

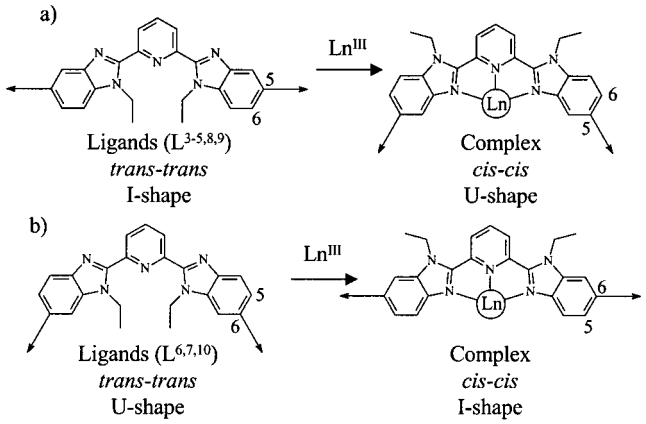

Figure 1. Conformational changes (trans-trans → cis-cis) occurring upon complexation to Ln(III) and related molecular anisometry observed for (a) 5-substituted ligands ($L^{3-5,8,9}$) and (b) 6-substituted ligands ($L^{6,7,10}$).

absence of mesomorphism to the reduced anisometry of the ligand strand.[8] However, the increased spatial expansion and polarization associated with the introduction of $Ln(NO_3)_3$ may also prevent the formation of mesophases, and we report in this paper the syntheses of ligands $L^{6,7}$, which are analogous to L^5, but with the semirigid lipophilic chains attached to the 6-positions. These ligands are programmed to adopt I-shaped arrangements upon complexation to Ln(III) (Figure 1b) and allow us to address the relative effects of anisometry, spatial expansion, and polarization on the thermal behavior of the final materials. Moreover, the effects of C- or O-substituted benzimidazole rings on the photophysical properties are investigated theoretically using semiempirical methods to obtain information that may be applicable to the development of new luminescent lanthanide-containing materials.

Experimental Section

General Information. Solvents and starting materials were purchased from Fluka AG (Buchs, Switzerland) and used without further purification, unless otherwise stated. Acetonitrile, dichloromethane, *N*,*N*-dimethylformamide (DMF), dimethyl sulfoxide (DMSO), and triethylamine were distilled from CaH_2. Chloroform was distilled from P_2O_5, methanol (MeOH) from $Mg(OMe)_2$, tetrahydrofuran (THF) from sodium, and thionyl chloride from elemental sulfur. 3,4-bis(dodecyloxy)benzoic acid (**9**), 4-(dodecyloxy)benzyl alcohol (**10**), and 4-(dodecyloxy)benzyl bromide (**12**) were obtained according to literature procedures.[8] The nitrate salts $Ln(NO_3)_3 \cdot nH_2O$ (Ln = La−Lu) were prepared from the corresponding oxides (Glucydur; 99.99%) according to literature procedures.[9] Silica gel (Merck 60; 0.040−0.060 mm) was used for preparative column chromatography.

Preparation of 3-Amino-4-nitroanisole (2). Sodium (2.0 g, 86.9 mmol) was dissolved in dry methanol (100 mL), and after 1 h of stirring, 3-amino-4-nitrochlorobenzene (**1**) (10.0 g, 57.9 mmol) was added. The resulting mixture was transferred into an autoclave and heated to 100 °C for 24 h. The solvent was evaporated, and the solid residue was partitioned between CH_2Cl_2 (100 mL) and water (50 mL). Hydrochloric acid (1 M) was added to neutralize the aqueous phase (pH = 6−7), the organic phase was removed, and the aqueous phase was extracted with dichloromethane (3 × 50 mL). The combined organic phases were dried (Na_2SO_4), filtered over silica (2 cm), and evaporated, and the residual solid was crystallized from CH_2Cl_2/hexane, giving 9.22 g (54.8 mmol, 94% yield) of **2** as red microcrystals. Mp: 125−126 °C. ^{1}H NMR in $CDCl_3$: δ 3.83 (3H, s), 6.15 (1H, d, ^4J = 2.5 Hz), 6.23 (1H, br s), 6.30 (1H, dd, ^3J = 9 Hz, ^4J = 2.5 Hz), 8.08 (1H, d, ^3J = 9 Hz). EI-MS: *m*/*z* 168.0 (M^+).

(8) Nozary, H.; Piguet, C.; Tissot, P.; Bernardinelli, G.; Deschenaux, R.; Vilches, M.-T. *Chem. Commun.* **1997**, 2101, 2249 (corrigendum). Nozary, H.; Piguet, C.; Tissot, P.; Bernardinelli, G.; Bünzli, J.-C. G.; Deschenaux, R.; Guillon, D. *J. Am. Chem. Soc.* **1998**, *120*, 12274.

(9) Desreux, J. F. In *Lanthanide Probes in Life, Chemical and Earth Sciences*; Bünzli, J.-C. G., Choppin, G. R., Eds.; Elsevier Publishing Co.: Amsterdam, 1989; Chapter 2.

Preparation of *N*-(5-Methoxy-2-nitrophenyl)acetamide (3). 3-Amino-4-nitroanisole (**2**) (3.2 g, 19 mmol) and triethylamine (8.55 mL, 6.21 g, 57 mmol) were dissolved in chloroform (50 mL) at 0 °C under an inert atmosphere, and acetyl chloride (5.4 mL, 5.96 g, 76 mmol) was slowly added. After completion of the reaction (reflux, 48 h, TLC; CH_2Cl_2/MeOH, 98:2), half-saturated aqueous NH_4Cl (30 mL) was added, the organic layer was removed, and the aqueous phase was extracted with dichloromethane (3 × 30 mL). The combined organic phases were dried (Na_2SO_4), filtered over silica (2 cm), and evaporated, and the residual solid was crystallized from CH_2Cl_2/hexane, giving 2.79 g (13.3 mmol, 70% yield) of **3** as pale yellow microcrystals. Mp: 123−125 °C. ^{1}H NMR in $CDCl_3$: δ 2.33 (3H, s), 3.91 (3H, s), 6.66 (1H, dd, ^3J = 9 Hz, ^4J = 2 Hz), 8.21 (1H, dd, ^3J = 9 Hz, ^4J = 2 Hz), 8.43 (1H, d, ^4J = 2 Hz). EI-MS: *m*/*z* 210.0 (M^+).

Preparation of *N*-Ethyl-(5-Methoxy-2-nitrophenyl)amine (4). N-(5-Methoxy-2-nitrophenyl)acetamide (**3**) (5.9 g, 28 mmol) was dissolved in dry dichloromethane (50 mL) at 0 °C under an inert atmosphere. A solution of diborane in THF (1 M, 60 mL, 60 mmol) was slowly added, and the resulting mixture was refluxed for 2 h. THF was distilled off, and excess diborane was destroyed with aqueous hydrochloric acid (1 M). The mixture was neutralized (pH = 7) with aqueous NaOH (1 M) and extracted with dichloromethane (3 × 100 mL). The combined organic phases were dried (Na_2SO_4) and evaporated, and the crude solid product was purified by column chromatography (silica gel; CH_2Cl_2), giving 2.65 g (13.5 mmol, 48% yield) of **4** as a pale yellow powder. Mp: 95−96 °C. ^{1}H NMR in $CDCl_3$: δ 1.38 (3H, t, ^3J = 7 Hz), 3.32 (2H, q, ^3J = 7 Hz), 3.88 (3H, s), 6.14 (1H, d, ^4J = 2.5 Hz), 6.23 (1H, dd, ^3J = 9 Hz, ^4J = 2.5 Hz), 8.15 (1H, d, ^3J = 9), 8.24 (1H, br s). EI-MS: *m*/*z* 196 (M^+).

Preparation of *N,N′*-Diethyl-*N,N′*-bis(5-methoxy-2-nitrophenyl)-pyridine-2,6-dicarboxamide (5). Pyridine-2,6-dicarboxylic acid (2.24 g, 12.6 mmol) and DMF (50 μL) were refluxed in freshly distilled thionyl chloride (40 mL) for 45 min under an inert atmosphere. Excess thionyl chloride was distilled from the reaction mixture, and the remainder was coevaporated with dry dichloromethane (2 × 20 mL) and dried under vacuum. *N*-Ethyl(5-methoxy-2-nitrophenyl)amine (**4**) (2.65 g, 12.6 mmol) and triethylamine (5.68 mL, 38 mmol) were mixed at 0 °C in dry dichloromethane (30 mL), and solid 2,6-dichlorocarboxypyridine, previously prepared, was added in three successive portions every 4 h. The resulting mixture was refluxed for 8 h, evaporated to dryness, and partitioned between dichloromethane (30 mL) and half-saturated aqueous NH_4Cl (30 mL), followed by extraction of the aqueous phase with dichloromethane (3 × 50 mL). The combined organic fractions were evaporated to dryness, and the crude product was purified by column chromatography (silica gel; CH_2Cl_2/MeOH, 99.8:0.2 → 99:1), giving 2.00 g (3.82 mmol, 60% yield) of **5** as a yellow powder. ^{1}H NMR in $CDCl_3$: δ 0.91−1.40 (6H, m), 3.80−3.95 (6H, m), 3.49−4.30 (4H, m), 6.60 (2H, d, ^4J = 3 Hz), 6.78 (2H, dd, ^3J = 9 Hz, ^4J = 3 Hz), 7.36 (2H, d, ^3J = 8 Hz), 7.84 (1H, t, ^3J = 8 Hz), 7.97 (2H, d, ^3J = 9 Hz). ES-MS: *m*/*z* 524.2 ($[M + H]^+$).

Preparation of 2,6-Bis(1-ethyl-6-methoxybenzimidazol-2-yl)-pyridine (6). *N,N′*-Diethyl-*N,N′*-bis(5-methoxy-2-nitrophenyl)pyridine-2,6-dicarboxamide (**5**) (2.0 g, 3.8 mmol) was dissolved in ethanol/water (350 mL/90 mL). Activated iron powder (4.26 g, 76.4 mmol) and concentrated hydrochloric acid (37%, 10.9 mL, 130 mmol) were added, and the mixture was refluxed for 12 h. Excess iron was filtered off, and ethanol was removed by vacuum distillation. The remaining mixture was poured into CH_2Cl_2 (200 mL), $Na_2H_2EDTA{\cdot}2H_2O$ (30 g) dissolved in water (300 mL) was added, and the resulting mixture was neutralized (pH = 8.5) with 24% aqueous NH_4OH under stirring. Concentrated hydrogen peroxide (30%, 9 mL) was then added under vigorous stirring. After 15 min, the organic layer was removed and the aqueous phase extracted with CH_2Cl_2 (3 × 40 mL). The combined organic phases were dried (Na_2SO_4) and evaporated, and the crude residue was purified by column chromatography (silica gel; CH_2Cl_2/MeOH, 98:2) and crystallized from CH_2Cl_2/hexane, giving 1.58 g (3.70 mmol, 96% yield) of **6** as white microcrystals. ^{1}H NMR in $CDCl_3$: δ 1.36 (6H, t, ^3J = 7 Hz), 3.93 (6H, s), 4.77 (4H, q, ^3J = 7 Hz), 6.90 (2H, d, ^3J = 2 Hz), 7.0 (2H, dd, ^3J = 9 Hz, ^4J = 2 Hz), 7.75 (2H, d, ^3J = 9 Hz), 8.01 (1H, t, ^3J = 8 Hz), 8.28 (2H, d, ^3J = 8 Hz). ES-MS: *m*/*z* 428.2 ($[M + H]^+$).

Preparation of 2,6-Bis(1-ethyl-6-hydroxybenzimidazol-2-yl)-pyridine (7). 2,6-Bis(1-ethyl-6-methoxybenzimidazol-2-yl)pyridine (**6**) (1.24 g, 2.9 mmol) was dissolved in dichloromethane (50 mL), and boron tribromide (1 M in CH_2Cl_2, 58 mL, 58 mmol) was added via a syringe under an inert atmosphere. After 4 h of stirring at room temperature, methanol (30 mL) was added and the resulting solution was evaporated to dryness. The solid residue was suspended in water (30 mL), and the pH was set to 13−14 with NaOH (5 M). The aqueous phase was extracted with dichloromethane (3 × 30 mL), and the extract was partially neutralized (pH = 10) with concentrated hydrochloric acid. The precipitate was filtered off, dried under vacuum, and recrystallized from CH_2Cl_2/MeOH (1:1), giving 1.12 g (2.80 mmol, 97% yield) of **7** as white microcrystals. Mp: >250 °C. ^{1}H NMR in DMSO-d_6: δ 1.26 (6H, t, ^3J = 7 Hz), 4.74 (4H, q, ^3J = 7 Hz), 6.80 (2H, dd, ^3J = 9 Hz, ^4J = 2 Hz), 6.94 (2H, d, ^4J = 2 Hz), 7.54 (2H, d, ^3J = 9 Hz), 8.13 (1H, t, ^3J = 7 Hz), 8.24 (2H, d, ^3J = 7 Hz), 9.50 (s, 2H). ES-MS: *m*/*z* 400.2 ($[M + H]^+$).

Preparation of 3,4-Bis(dodecyloxy)benzyl Alcohol (11). $LiAlH_4$ (84 mg, 2.24 mmol) was dissolved in dry tetrahydrofuran (50 mL), and 3,4-bis(dodecyloxy)benzoic acid (**9**) (550 mg, 1.12 mmol) dissolved in tetrahydrofuran (10 mL) was slowly added under an inert atmosphere. The resulting mixture was refluxed for 24 h. Excess $LiAlH_4$ was destroyed with water (20 mL), and the resulting heterogeneous mixture was evaporated to dryness and partitioned between CH_2Cl_2 (100 mL) and water (20 mL). The aqueous phase was acidified (pH = 2) with aqueous hydrochloric acid (1 M). The organic layer was then carefully removed, and the aqueous phase was extracted with dichloromethane (3 × 30 mL). The combined organic phases were filtered, dried (Na_2SO_4), and evaporated, and the crude product was crystallized from CH_2Cl_2/hexane, giving 494 mg (1.04 mmol, 92% yield) of **11** as a white powder. Mp: 54 °C. ^{1}H NMR in $CDCl_3$: δ 0.84 (3H, t, ^3J = 7 Hz), 1.2 (36H, m), 1.8 (4H, m), 3.94 (2H, t, ^3J = 7 Hz), 3.97 (2H, t, ^3J = 7 Hz), 4.56 (2H, s), 6.80 (2H, d, ^3J = 9 Hz), 6.78 (2H, s), 6.85 (1H, s). EI-MS: *m*/*z* 476 (M^+).

Preparation of 3,4-Bis(dodecyloxy)benzyl Bromide (13). 3,4-Bis(dodecyloxy)benzyl alcohol (**11**) (480 mg, 1.0 mmol) and phosphorus tribromide (545 mg, 2.0 mmol) were refluxed for 15 h in dichloromethane (50 mL). Excess PBr_3 was hydrolyzed with half-saturated aqueous NaCl (20 mL), and the organic layer was removed. The aqueous phase was extracted with dichloromethane (3 × 30 mL), and the combined organic phases were filtered over silica (2 cm), dried (Na_2SO_4), and evaporated. The crude product was crystallized from CH_2Cl_2/hexane, giving 496 mg (0.91 mmol, 91% yield) of **13** as white microcrystals. Mp: 65−66 °C. ^{1}H NMR in $CDCl_3$: δ 0.84 (3H, t, ^3J = 7 Hz), 1.2 (36H, m), 1.8 (4H, m), 3.94 (2H, t, ^3J = 7 Hz), 3.95 (2H, t, ^3J = 7 Hz), 4.49 (2H, s), 6.76 (2H, d, ^3J = 8 Hz), 6.87 (1H, s), 6.90 (2H, d, ^3J = 8 Hz). EI-MS: *m*/*z* 540/538 (M^+).

Preparation of 2,6-Bis[1-ethyl-6-((4-(dodecyloxy)benzyl)oxy)benzimidazol-2-yl]pyridine (L^6). NaH (50% in oil, 96 mg, 2.0 mmol) was added to a solution of 2,6-bis(1-ethyl-6-hydroxybenzimidazol-2-yl)-pyridine (**7**) (400 mg, 1.0 mmol) in dry *N,N′*-dimethylformamide (50 mL) at 0 °C. An orange precipitate was immediately observed, and the solution was stirred for 1 h. 4-(Dodecyloxy)benzyl bromide (**12**) (711 mg, 2.0 mmol) was added in one portion, and the resulting mixture was heated at 100 °C for 24 h. After the mixture was cooled to room temperature, water (200 mL) was added and the resulting precipitate was filtered off, washed with water, and dried under vacuum. The residual solid was dissolved in dichloromethane (50 mL), and the solution was washed with half-saturated aqueous NaCl (50 mL). The organic layer was removed, and the aqueous phase was extracted with dichloromethane (2 × 50 mL). The combined organic phases were dried (Na_2SO_4) and evaporated, and the crude product was purified by column chromatography (silica gel; CH_2Cl_2/MeOH, 100:0 → 99:1) and crystallized from propionitrile, giving 900 mg (0.95 mmol, 94% yield) of $\mathbf{L}^6$ as white microcrystals. Mp: 154 °C. ^{1}H NMR in $CDCl_3$: δ 0.88 (6H, t, ^3J = 7 Hz, $CH_3{-}C_{11}H_{22}O$), 1.27 (36 H, br s, $CH_3{-}C_9H_{18}{-}C_2H_4O$), 1.34 (6H, t, ^3J = 7 Hz, $CH_3{-}CH_2{-}N$), 1.79 (4H, m, $C_{10}H_{21}{-}CH_2{-}CH_2O$), 3.97 (4H, t, ^3J = 7 Hz, $C_{11}H_{23}{-}CH_2O$), 4.75 (4H, q, ^3J = 7 Hz, $CH_3{-}CH_2{-}N$), 5.09 (4H, s, $H^{10,11}$), 6.94 (4H, d, ^3J = 9 Hz, $H^{6,6'}$), 6.99 (2H, d, ^4J = 2 Hz, H^3), 7.06 (2H, dd, ^3J = 9 Hz, ^4J = 2 Hz, H^4), 8.01 (1H, t, ^3J = 8 Hz, H^1), 8.29 (2H, d, ^3J = 8 Hz, H^2), 8.40 (4H, d, ^3J = 9 Hz, H^7), 8.76 (2H, d, ^3J = 9 Hz, H^5). ^{13}C NMR in $CDCl_3$: δ

14.3, 15.4 (primary C); 22.9, 26.2, 29.4, 29.5, 29.6, 29.8, 32.1, 39.9, 68.2, 70.9 (secondary C); 95.1, 113.2, 114.8, 121.0, 125.3, 129.5, 138.2 (tertiary C); 128.8, 136.7, 137.7, 149.5, 150.0, 156.6, 159.3 (quaternary C). ES-MS: *m*/*z* 948.5 ($[M + H]^+$).

Preparation of 2,6-Bis[1-ethyl-6-((3,4-bis(dodecyloxy)benzyl)oxy)-benzimidazol-2-yl]pyridine (L^7). The same procedure as that for L^6 was used, starting from 3,4-bis(dodecyloxy)benzyl bromide (**13**) and **7**. Yield: 77%. Mp: 74 °C. ^{1}H NMR in $CDCl_3$: δ 0.83 (6H, t, ^3J = 7 Hz, $CH_3-C_{11}H_{22}O$), 0.84 (6H, t, ^3J = 7 Hz, $CH_3-C_{11}H_{22}O$), 1.27 (72 H, br s, $CH_3-C_9H_{18}-C_2H_4O$), 1.30 (6H, t, ^3J = 7 Hz, CH_3-CH_2-N), 1.78 (8H, m, $C_{10}H_{21}-CH_2-CH_2O$), 3.96 (4H, t, ^3J = 7 Hz, $C_{11}H_{23}-CH_2O$), 3.98 (4H, t, ^3J = 7 Hz, $C_{11}H_{23}-CH_2O$), 4.71 (4H, q, ^3J = 7 Hz, CH_3-CH_2-N), 5.03 (s, 4H, $H^{10,11}$), 6.86 (2H, d, ^3J = 8 Hz, H^6), 6.94 (2H, br s, $H^{6'}$), 6.96 (2H, d, ^3J = 8 Hz, H^7), 6.99 (2H, d, ^4J = 2 Hz, H^3), 7.03 (2H, dd, ^3J = 9 Hz, ^4J = 2 Hz, H^4), 7.72 (2H, d, ^3J = 9 Hz, H^5), 7.97 (1H, t, ^3J = 8 Hz, H^1), 8.24 (2H, d, ^3J = 8 Hz, H^2). ^{13}C NMR in $CDCl_3$: δ 14.3, 15.4 (primary C); 22.9, 26.2, 29.4, 29.5, 29.6, 29.8, 29.9, 32.1, 39.9, 69.4, 69.5, 71.2 (secondary C); 95.1, 113.8, 113.9, 120.7, 121.0, 125.3 (tertiary C); 129.5; 136.7, 137.7, 138.1, 149.3, 150.0, 156.6 (quaternary C). ES-MS: *m*/*z* 1317.4 ($[M + H]^+$).

Preparation of $[Ln(L^i)(NO_3)_3]\cdot xH_2O$ (i = 6, 7) and $[Ln(L^6)(CF_3CO_2)_3]_2\cdot xH_2O$. L^i (i = 6, 7) (0.053 mmol) samples in dichloromethane (5 mL) were added to $Ln(NO_3)_3\cdot xH_2O$ (x = 2−6) (0.053 mmol) or $Ln(CF_3CO_2)_3\cdot xH_2O$ (x = 1−2) (0.053 mmol) in acetonitrile (5 mL). After 1 h of stirring at room temperature, the solvents were evaporated to dryness and the residual solids were solubilized in hot acetonitrile. Cooling the solutions produced white powders, which were further recrystallized from acetonitrile, propionitrile, or isobutyronitrile, giving 75−91% yields of the complexes $[Ln(L^6)(NO_3)_3]\cdot xH_2O$ (Ln = La, x = 0, **14**; Eu, x = 0, **15**; Gd, x = 1, **16**; Tb, x = 0, **17**; Lu, x = 0, **18**), $[Ln(L^7)(NO_3)_3]\cdot xH_2O$ (Ln = La, x = 0, **19**; Eu, x = 0, **20**; Lu, x = 1, **21**), and $[Ln(L^6)(CF_3CO_2)_3]_2\cdot xH_2O$ (Ln = La, x = 3, **22**; Lu, x = 0, **23**). X-ray-quality crystals of $[Lu(L^6)(NO_3)_3]\cdot CH_3CN$ (**18a**) and $[Ln(L^6)(CF_3CO_2)_3]_2$ (**23**) were obtained with the same procedure, and the crystals were directly transferred from their mother liquors to the diffractometer. Complexes **14**−**23** were characterized by their IR spectra and gave satisfactory elemental analyses (Table S1, Supporting Information).

Physicochemical Measurements. Reflectance spectra of the samples as finely ground powders dispersed in MgO (5%) were recorded with MgO as reference on a Perkin-Elmer Lambda 900 spectrophotometer equipped with a PELA-1000 integration sphere from Labsphere. Electronic spectra in the UV−visible range were recorded at 20 °C from 10^{-3}−10^{-4} M CH_2Cl_2/MeCN solutions with Perkin-Elmer Lambda 5 and Lambda 900 spectrometers using quartz cells of 0.1 and 1 cm path lengths. IR spectra were obtained from KBr pellets with a Perkin-Elmer 883 spectrometer. ^{1}H and ^{13}C NMR spectra were recorded at 25 °C on a Varian Gemini 300 broad-band spectrometer. Chemical shifts are given in ppm with reference to TMS. EI mass spectra (70 eV) were recorded with VG 7000E and Finnigan 4000 instruments. Pneumatically assisted electrospray (ES) mass spectra were recorded from CH_2Cl_2 solutions on a Finnigan MAT SSQ 7000 and on an API III tandem mass spectrometer (PE Sciex). The spectra were recorded under low up-front declustering or collision-induced-dissociation (CID) conditions; typically, ΔV was 0−30 V between the orifice and the first quadrupole of the spectrometer.[8] The experimental procedures for high-resolution laser-excited luminescence measurements have been published previously.[7] Solid-state samples were finely powdered, and low temperature (77 or 10 K) was achieved by means of a Cryodyne model 22 closed-cycle refrigerator from CTI Cryogenics. Luminescence spectra were corrected for the instrumental function; excitation spectra were not. Lifetimes are averages of at least three to five independent determinations. Ligand excitation and emission spectra were recorded on a Perkin-Elmer LS-50B spectrometer equipped for low-temperature measurements. DSC traces were obtained with a Seiko DSC 220C differential-scanning calorimeter from 3−5 mg samples (5−10 °C·min^{-1}, under N_2). Thermogravimetric analyses were performed with a Seiko TG/DTA 320 thermogravimetric balance (under N_2). The characterizations of the mesophases were performed with a Leitz Orthoplan-Pol polarizing microscope equipped with a Leitz LL 20×/0.40 polarizing objective and a Linkam THMS 600 variable-temperature stage.

Scheme 1[a]

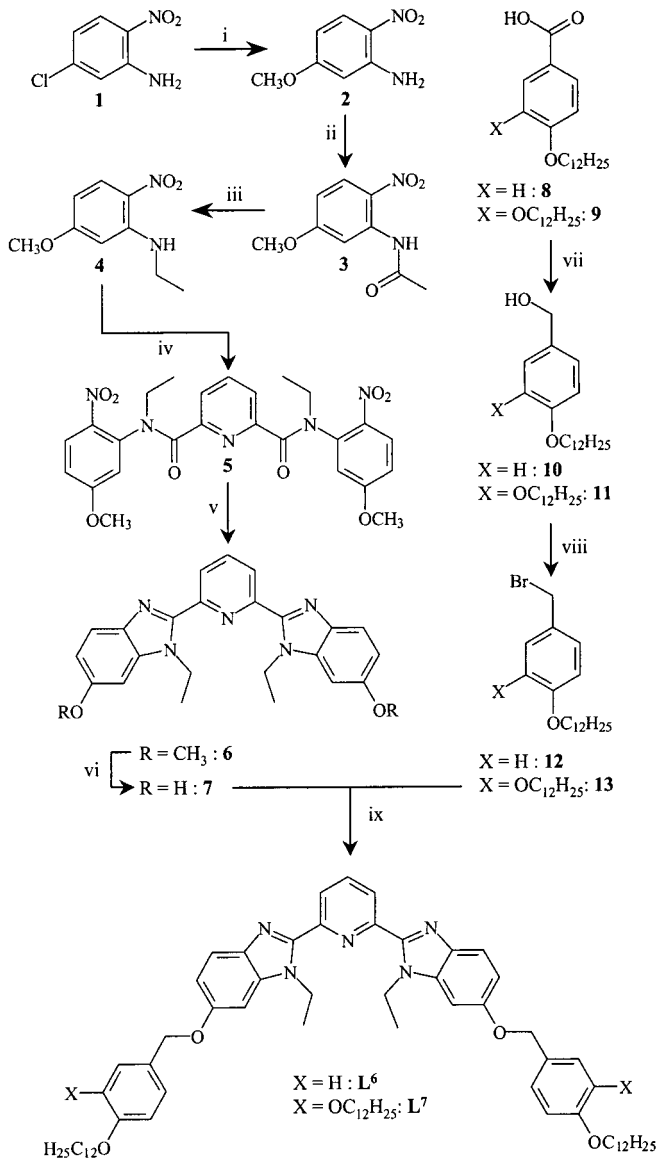

[a] *Reagents*: (i) MeONa/MeOH; (ii) CH_3COCl, NEt_3, $CHCl_3$; (iii) B_2H_6, THF; (iv) 2,6-pyridinedicarbonyldichloride, NEt_3, CH_2Cl_2; (v) Fe, HCl, EtOH, H_2O; (vi) BBr_3, CH_2Cl_2; (vii) $LiAlH_4$, THF; (viii) PBr_3, CH_2Cl_2; (ix) NaH, DMF.

Elemental analyses were performed by Dr. H. Eder at the Microchemical Laboratory of the University of Geneva.

X-ray Crystal Structure Determinations of $[Lu(L^6)(NO_3)_3]\cdot CH_3CN$ (18a) and $[Ln(L^6)(CF_3CO_2)_3]_2$ (23). A summary of the crystal data, intensity measurements, and structure refinements are reported in Table 1. Data were collected at 200 K on a STOE STADI4 diffractometer ($\omega-2\theta$ scan; scan width = (1.05 + 0.35 tan θ)°; scan speed 0.06° s^{-1}; Cu Kα radiation, λ = 1.5418 Å). Two reference reflections, measured every 45 min (**18a**) or 60 min (**23**), showed no significant variations. Data were corrected for Lorentz, polarization, and absorption effects.[10] The structures were solved by direct methods using MULTAN 87;[11] all other calculations used the XTAL[12] system and ORTEP II[13] programs. Full-matrix least-squares refinements (on *F*) were performed. The non-H atoms were refined with anisotropic displacement parameters. H atoms were placed in calculated positions and contributed to F_c calculations.

Results and Discussion

Syntheses of Ligands $L^{6,7}$ (Scheme 1). The lipophilic ligands L^6 and L^7 are prepared according to a convergent strategy in

Table 1. Summary of Crystal Data, Intensity Measurements, and Structure Refinement Details for $[Lu(L^6)(NO_3)_3]\cdot CH_3CN$ (**18a**) and $[Lu(L^6)(CF_3CO_2)_3]_2$ (**23**)

	18a	**23**
	$[Lu(L^6)(NO_3)_3]\cdot CH_3CN$	$[Lu(L^6)(CF_3CO_2)_3]_2$
formula	$LuC_{63}H_{84}N_9O_{13}$	$Lu_2C_{134}H_{162}N_{10}O_{20}F_{18}$
mol wt	1350.4	2924.7
cryst syst	monoclinic	triclinic
space group	$P2_1/n$	$P\bar{1}$
a, Å	9.726(3)	13.964(3)
b, Å	19.081(3)	14.217(3)
c, Å	34.639(3)	18.661(2)
α, deg	90	110.60(1)
β, deg	90.279(8)	102.78(2)
γ, deg	90	97.88(1)
V, Å^3	6428(2)	3287(1)
Z	4	1
D_{calc}, g·cm^{-3}	1.395	1.478
F(000)	2800	1500
$\lambda_{Cu\ K\alpha}$, Å	1.5418	1.5418
$\mu_{Cu\ K\alpha}$, mm^{-1}	3.499	3.618
abs: A^*_{min}/A^*_{max}	1.180/3.039	1.358/2.869
cryst size, mm	0.046 × 0.29 × 0.54	0.09 × 0.24 × 0.40
temp, K	200	200
no. of reflns measd	8009	8370
θ range, deg	$2 < 2\theta < 108$	$2 < 2\theta < 110$
hkl ranges	$-10 < h < 10$	$-14 < h < 14$
	$0 < k < 20$	$-14 < k < 14$
	$0 < l < 36$	$0 < l < 19$
no. of unique refln	7857	8062
no. of obs reflns ($\|F_o\| > 4\sigma(F_o)$)	5325	6537
no. of variables	776	830
R	0.062	0.055
w	$1/(\sigma^2(F_o) + 0.0002(F_0)^2)$	$1/(\sigma^2(F_o) + 0.0001(F_o)^2)$
R_w[a]	0.054	0.048
S	1.52(2)	1.68(2)
max Fourier diff, e·Å^{-3}	−1.03, 0.94	−1.19, 1.97

[a] $R_w = [\sum w(|F_o| - |F_c|)^2/\sum w|F_o|^2]^{0.5}$.

which the semilipophilic sidearms **12** and **13** are attached to the 6-position of the dihydroxy binding unit **7** via nucleophilic displacements. The latter synthon **7** is obtained by a multistep synthesis using a modified Phillips reaction as the key step,[14] which provides two benzimidazole rings in **6** via the reduction and cyclization of the symmetrical bis(*o*-nitroarenecarboxamide) **5**. A similar approach was previously developed for the analogous ligands L[5,8], but the introduction of a *p*-methoxy group into **4** was less trivial since *p*-methoxy-*o*-chloronitrobenzene is not commercially available. We thus resort to **1** as the starting material, which undergoes a nucleophilic aromatic substitution to give **2**. Monoalkylation of the poorly nucleophilic *o*-nitro arene amine is achieved by a two-step acylation−reduction process in which the amide group is selectively reduced by diborane in the presence of nitro groups.[15] The ^{1}H and ^{13}C NMR spectra of L^6[6,7] confirm the proposed structures, and the systematic absence of NOE effects between the methylene protons (H^{8,9}) and the pyridine proton H^2 is the signature of a trans-trans conformation of the tridentate unit in solution on the NMR time scale (average C_{2v}), as previously demonstrated for L^5 in solution and in the solid state.[8]

(10) Blanc, E.; Schwarzenbach, D.; Flack, H. D. *J. Appl. Crystallogr.* **1991**, *24*, 1035.
(11) Main, P.; Fiske, S. J.; Hull, S. E.; Lessinger, L.; Germain, D.; Declercq, J. P.; Woolfson, M. M. MULTAN 87. Universities of York, England, and Louvain-La-Neuve, Belgium, 1987.
(12) Hall, S. R., Flack, H. D., Stewart, J. M., Eds. *XTAL 3.2 User's Manual*; Universities of Western Australia and Maryland: Nedlands, Australia, and College Park, MD, 1992.
(13) Johnson, C. K. *ORTEP II*; Report ORNL-5138; Oak Ridge National Laboratory: Oak Ridge, TN, 1976.
(14) Piguet, C.; Bocquet, B.; Hopfgartner, G. *Helv. Chim. Acta* **1994**, *77*, 931.
(15) Brown, H. C.; Heim, P. *J. Org. Chem.* **1973**, *38*, 912.

Table 2. Ligand-Centered Absorptions and Emission Properties of Ligands L[3,5,6] (10^{-5} M in CH_3CN/CH_2Cl_2 (7:3)) and the Complexes $[Ln(L^6)(NO_3)_3]$ (**14**−**18**) (10^{-4} M in CH_3CN) at 298 K[a]

compound	absorption, cm^{-1} $\pi \rightarrow \pi^*$	emission, cm^{-1} $^1\pi\pi^*$	λ_{exc}, nm
L^3	33 900 (30 900 sh)	26 740	328
	31 050 (40 100)		
L^5	38 460 (7230 sh)	23 980	345
	36 230 (11 470)		
	28 570 (30 830)		
L^6	39 060 (13 900 sh)	24 630	337
	29 670 (37 600)		
$[La(L^6)(NO_3)_3]$ (**14**)	29 585 (22 800 sh)	20 350	400
	27 320 (24 800)		
$[Gd(L^6)(NO_3)_3]$ (**16**)	29 585 (27 500 sh)	20 490	407
	26 740 (30 300)		
$[Lu(L^6)(NO_3)_3]$ (**18**)	29 760 (27 600)	19 230	419
	26 315 (29 300)		
$[Eu(L^6)(NO_3)_3]$ (**15**)	29 675 (24 600 sh)	b	
	27 030 (26 900)		
$[Tb(L^6)(NO_3)_3]$ (**17**)	29 675 (26 000 sh)	b	
	26 665 (28 000)		

[a] Energies are given for the maxima of the band envelopes in cm^{-1}, and the molar absorption coefficients (ϵ) are given in parentheses in M^{-1}·cm^{-1}; sh = shoulder. [b] Not detected due to L$^6 \rightarrow$ Ln(III) energy transfer.

Photophysical Properties and Electronic Structures of Ligands L$^{3-10}$. Except for a better resolution in solution, the absorption spectra of the ligands L^3, L^5, and L^6 are similar for samples in solution (transmission, Table 2) and in the solid state (reflectance, Table 3), which strongly supports a common trans-trans conformation for the tridentate binding units of all ligands in both states. The UV spectrum of L^3 is dominated by an

Table 3. Ligand-Centered Absorption and Emission Properties of Ligands $L^{3,5,6}$ and the Complexes $[Ln(L^6)(NO_3)_3]$ (**14**−**18**) in the Solid State[a]

compd	absorption, cm^{-1} $\pi \rightarrow \pi^*$ + $n \rightarrow \pi^*$	emission, cm^{-1}		lifetime, ms
		$^1\pi\pi^*$	$^3\pi\pi^*$	$\tau(^3\pi\pi^*)$
L^3	38 460 sh	27 320 sh	20 410	415(5)
	32 470	26 455	18 350	
	28 330	25 060 sh	17 120	
L^5	39 000 sh	26 180 sh	20 700	592(10)
	32 260 sh	25 380	19 450 sh	
	26 920	24 880	18 180 sh	
		24 100		
L^6	29 850	26 100 sh	19 725	315(6)
	27 027 sh	25 000	18 350	
		23 585	16 810	
		22 200 sh		
$[La(L^6)(NO_3)_3]$ (**14**)	27 780	22 400	19 610	111(1)
	25 000 sh		18 020	
$[Gd(L^6)(NO_3)_3]$ (**16**)	27 400	*b*	19 230	1.33(1)
	24 690 sh		17 700	
			16 530	
$[Lu(L^6)(NO_3)_3]$ (**18**)	27 400	22 370	19 230	57.1(4)
	24 600 sh	21 230	17 700	
			16 530	
$[Eu(L^6)(NO_3)_3]$ (**15**)	27 400	*c*	*c*	*c*
	25 000 sh			

[a] Reflectance spectra recorded at 295 K, luminescence data at 77 K, and lifetime measurements at 10 K (λ_{exc} = 308 nm); sh = shoulder. [b] Too weak to be measured. [c] $^1\pi\pi^*$ or $^3\pi\pi^*$ luminescence quenched by transfer to the Ln ion.

intense, broad, and asymmetric band centered at 31 050 cm^{-1}, which is red-shifted by 2480 cm^{-1} (L^5) and 1290 cm^{-1} (L^6) when π-donor oxygen atoms are attached to the benzimidazole ring (Table 2, Figure 4). Previous EHMO calculations on 2,6-bis(1-methylbenzimidazol-2-yl)pyridine ligands (L^2, R^1 = Me, R^2 = H) in the trans-trans conformation (C_{2v} symmetry) suggest that (i) the main component of this transition can be assigned to $\pi_1(A_2) \rightarrow \pi^*(B_1)$ and (ii) π-donor groups bound to the 5-positions of the benzimidazole rings destabilize the $\pi_1(A_2)$ level, which accounts for the red shift of the main transition.[16] However, these predictions result from calculations involving methyl groups bound to the 5-positions, and we have resorted to semiempirical methods to further extend this approach for ligands bearing carbon or oxygen atoms connected to the benzimidazole rings. Starting from the X-ray crystal structure of L^8 (trans-trans conformation),[8] The gas-phase geometry has been optimized by using the PM3 method.[17] As far as its central semirigid core is concerned, L^8 is a good model for L^3, which limits excessive computing, and we have interconverted the methylene unit and oxygen atom of the bridges to produce L^9 as a model for L^5. Finally, shifting the $-O-CH_2-$ bridges from the 5-position in L^9 to the 6-position in L^{10} provides a valuable model for L^6.

After having tested the semiempirical ZINDO method[18] by calculating the electronic structures and singlet−singlet electronic transitions for pyridine, pyrimidine, pyrazine, benzene, and naphthalene moieties and comparing the results with those found in ref 19, we computed the ground-state orbitals of L^{8-10} in their PM3 optimized geometries (Figures S1-S6, Supporting Information). For all studied ligands, the frontier orbitals (HOMO and LUMO) together with at least the next five orbitals at higher (SLUMO etc.) or at lower (SHOMO etc.) energies display π-character and the expected electronic transitions at low energy are of the $\pi \rightarrow \pi^*$ type. We systematically observe delocalized π-orbitals which involve either the tridentate 2,6-bis(benzimidazol-2-yl)pyridine core or the lateral phenyl rings, demonstrating the "insulating" effect of the two atoms of the $-CH_2-O-$ spacers in L^{8-10} (Figures 2 and 3). The HOMO and SHOMO of L^8 are localized on the 4-alkoxyphenol sidearms in agreement with the low oxidation potentials found for 1,4-dialkoxybenzenes,[20] and the next two filled π-orbitals at lower energies are centered on the tridentate binding unit (symmetric (119) and antisymmetric (118) with respect to the pseudo-2-fold axis bisecting the pyridine ring). ZINDO calculations predict that the $\pi \rightarrow \pi^*$ band envelope at lowest energy is formed by a combination of transitions centered on the tridentate

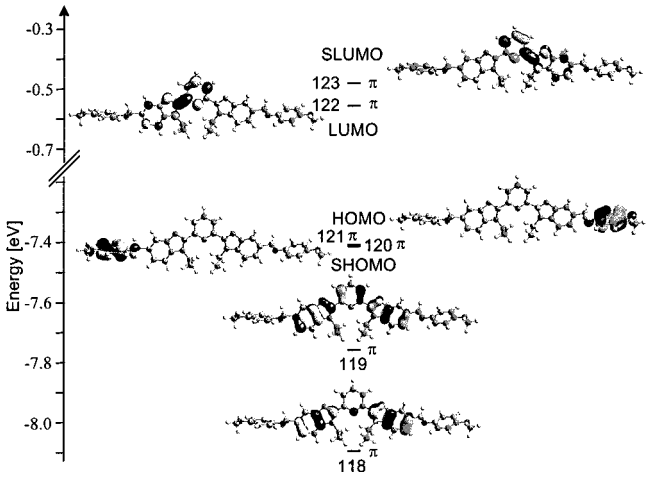

Figure 2. Schematic representation of selected frontier orbitals calculated with ZINDO[18] for L^8. Energies are given in eV (1 eV = 8065.5 cm^{-1}).

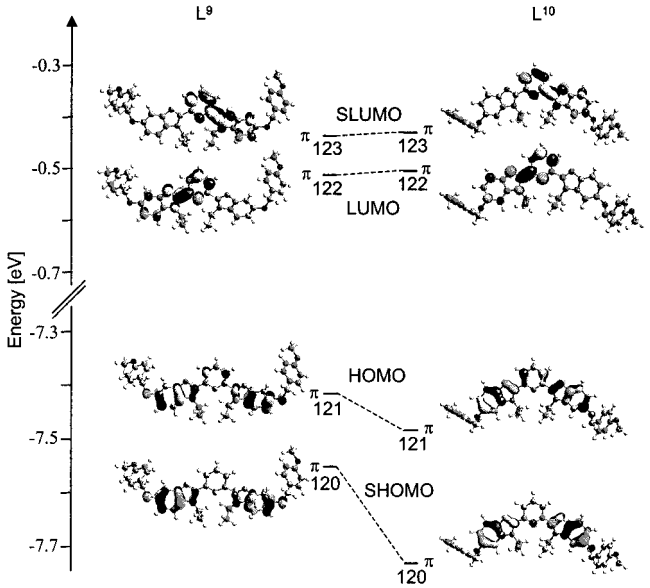

Figure 3. Walsh diagram for selected frontier orbitals calculated with ZINDO[18] for L^9 and L^{10}. Energies are given in eV (1 eV = 8065.5 cm^{-1}).

(16) Piguet, C.; Bünzli, J.-C. G.; Bernardinelli, G.; Bochet, C. G.; Froidevaux, P. *J. Chem. Soc., Dalton Trans.* **1995**, 83.
(17) Stewart, J. J. P. *J. Comput. Chem.* **1989**, *10*, 209, 221.
(18) Zerner, M. C. *ZINDO Manual*; QTP, University of Florida: Gainesville, FL, 1990. Broo, A.; Pearl, G. M.; Zerner, M. C. *J. Phys. Chem.* **1997**, *101*, 2478. Siegbahn, P. E.; Heidberg, A.; Roos, B. O.; Levy, B. *Phys. Ser.* **1980**, *21*, 323.
(19) Pearl, G. M.; Zerner, M. C.; Broo, A.; McKelvey, J. *J. Comput. Chem.* **1998**, *19*, 781.
(20) Effenberger, F.; Kottmann, H. *Tetrahedron* **1985**, *41*, 4171. Mattes, S. L.; Farid, S. *J. Am. Chem. Soc.* **1982**, *104*, 1454.

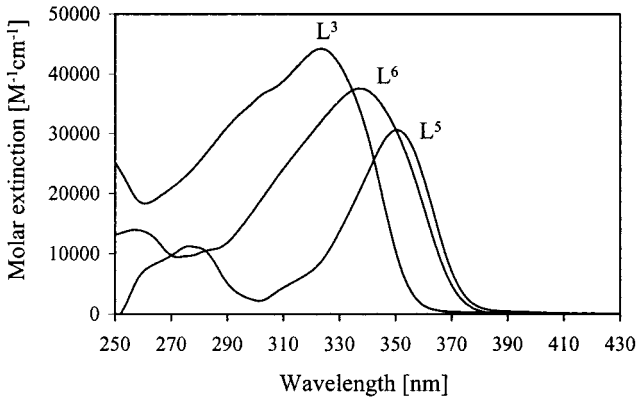

Figure 4. Absorption spectra of L^3, L^5, and L^6 (10^{-5} M) in CH_3CN/CH_2Cl_2 (7:3) at 298 K.

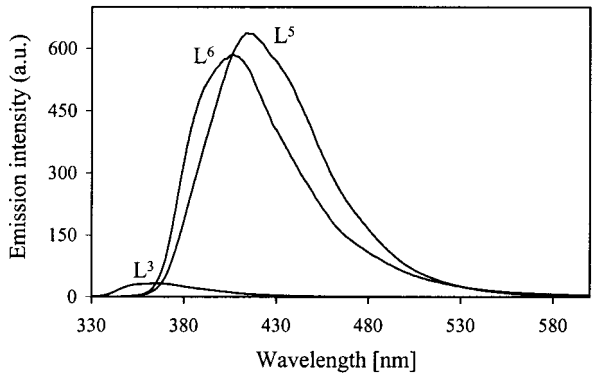

Figure 5. Emission spectra of L^3, L^5, and L^6 (10^{-5} M) in CH_3CN/CH_2Cl_2 (7:3) at 298 K. λ_{exc} values are given in Table 2.

core (118 → 123, 119 → 122, and 119 → 123) and occurring around 30 770 cm^{-1} (325 nm), in good agreement with the maximum of the experimental band envelopes observed for L^8 (30 960 cm^{-1}) and L^3 (31 050 cm^{-1}) in solution (Figure 4).[8]

ZINDO calculations obtained for PM3 optimized ligands L^9 and L^{10} show significant differences resulting from the direct connections of oxygen atoms to the 5-, and the 6-positions, respectively, of the benzimidazole rings (Figure 3). Compared to the case of L^8, the π-antibonding interactions between the oxygen atoms of the spacers and the carbon atoms of the benzimidazole rings to which they are connected destabilize the orbitals centered on the tridentate core, which become the HOMO and SHOMO of the system. As the orbitals of the oxygen atoms do not significantly affect the LUMO and SLUMO, reduced HOMO−LUMO gaps are expected for $L^{9,10}$ and we predict $\pi \rightarrow \pi^*$ transitions centered on the tridentate cores at lower energies for L^9 (29 420 cm^{-1}) and L^{10} (30 175 cm^{-1}), in qualitative good agreement with the maxima of the band envelopes found for L^5 (28 570 cm^{-1}) and L^6 (29 670 cm^{-1}) (Table 2, Figure 4). We thus assign the red shifts observed for $L^{5,6}$ compared to L^3 to the destabilization of the HOMOs resulting from the connection of π-donor oxygen atoms to the benzimidazole rings. Interestingly, the slightly larger destabilization of the HOMO and SHOMO predicted for 5-substituted benzimidazole rings in L^9 (compared to L^{10}, Figure 3) is supported by the experimental absorption spectrum of L^5, for which the maximum of the lowest $\pi \rightarrow \pi^*$ transition is red-shifted by 1100 cm^{-1} compared to that of L^6 (Table 2).

The emission spectra of L^3, L^5, and L^6 in solution (Figure 5) display broad and Stokes-shifted bands originating from the $^1\pi\pi^*$ level[8] and whose energies (26 740 cm^{-1} (L^3), 23 980 cm^{-1} (L^5), 24 630 cm^{-1} (L^6)) follow the expected order $L^3 \gg L^6 > L^5$ deduced from the absorption spectra and theoretically supported by ZINDO calculations. The ∼50-fold decrease in fluorescence from $L^{5,6}$ to L^3 has been ascribed to partial quenching by photoinduced-electron-transfer (PET) processes involving the easily oxidized 4-alkoxyphenol sidearms in L^3 which are absent in $L^{5,6}$.[8] The excitation spectra of $L^{3,5,6}$ recorded during the analysis of $^1\pi\pi^*$ emissions closely match the corresponding absorption spectra, which implies similar UV-harvesting properties for all studied ligands. The emission spectra of $L^{3,5,6}$ in the solid state (77 K) display structured $^1\pi\pi^*$ emission bands at energies comparable to those found in solution (0−0 phonon transitions, Table 3). Time-resolved spectra (delay 0.1−0.8 ms) reveal faint, but structured and long-lived, phosphorescence of $^3\pi\pi^*$ levels around 19 700−20 700 cm^{-1} (0−0 phonon transitions, τ = 300−600 ms, Table 3). We do not observe a straightforward correlation between the energies of $^1\pi\pi^*$ and $^3\pi\pi^*$ levels in these ligands, but the energies of the triplet states slightly decrease in the order $L^5 > L^3 > L^6$, which has a drastic effect on the luminescence of lanthanide complexes, since $^3\pi\pi^*$ states are involved in the sensitization process (vide infra).[21]

Thermal Behavior of Ligands $L^{3,5-7}$. The mesomorphic properties of L^3 and L^5 have been previously discussed and correspond to the formation of enantiotropic smectic A (S_A) phases together with monotropic smectic C (S_C) phases.[8] The shifts of the semilipophilic (4-(dodecyloxy)benzyl)oxy chains from the 5-positions in L^5 to the 6-positions in L^6 prevent mesomorphism, and thermal analyses by differential-scanning calorimetry (DSC) and polarizing microscopy show a single endothermic process occurring at 154 °C and corresponding to the isotropization. The attachment of a second dodecyloxy residue in L^7 does not restore mesomorphism, but it decreases the melting point by 80 °C (Table 4). As expected, the enthalpic term $\Delta H_{melting}$ increases from L^6 to L^7 because of the larger molecular weight of the latter compound, and the sharp decrease of the melting point has thus a pure entropic origin associated with the presence of a larger number of lipophilic alkyl chains (Table 4). Interestingly, a strict analogue of L^6 for which dodecyloxy ($OC_{12}H_{25}$) chains are replaced by docosyloxy ($OC_{22}H_{45}$) chains possesses a molecular weight similar to L^7 but it exhibits isotropization at 146 °C (ΔH = 64 kJ/mol, ΔS = 152 J/(mol·K)), which strongly suggests that the large entropic contribution observed for L^7 results from an increased organization of the crystalline phases to accommodate supplementary flexible alkyl chains. This is confirmed by the analogue of L^7 in which the semilipophilic sidearms are connected to the 5-positions (as in L^5), which displays isotropization at 124 °C (ΔH = 97 kJ/mol, ΔS = 244 J/(mol·K)) and no mesomorphism. Since we have established by electronic spectroscopy and X-ray diffraction that the tridentate binding units adopt similar trans-trans conformations in all ligands,[8] the major difference between L^5 and L^6 corresponds to a change from an I-shaped rodlike arrangement for L^5 to a U-shaped arrangement for L^6. X-ray crystal structures together with CPK models predict molecular anisotropies (length:width ratios) of ∼10 for L^5 [8] and only 1.2 for L^6 possessing (i) an approximately planar arrangement of the aromatic cores and (ii) all-trans conformations of the alkyl chains. The smectogenic behavior of L^5 indicates that a minimum axial anisometry is required, but the balance between the volumes of aromatic cores and flexible side chains is tricky, as demonstrated by the removal of mesomorphism for the analogue of L^5 bearing two supplementary flexible alkyl chains.

(21) Bünzli, J.-C. G.; Froidevaux, P.; Piguet, C. *New J. Chem.* **1995**, *19*, 661.

Table 4. Phase-Transition Temperatures and Enthalpy and Entropy Changes for Ligands $L^{3,5-7}$ and Thermal Behavior of the Complexes $[Ln(L^6)(NO_3)_3]\cdot xH_2O$ (**14**−**18**), $[Ln(L^7)(NO_3)_3]\cdot xH_2O$ (**19**−**21**), and $[Ln(L^6)(CF_3CO_2)_3]_2\cdot xH_2O$ (**22**−**23**)

compd	transition[a]	*T*, °C	ΔH, kJ·mol^{-1}	ΔS, J·mol^{-1}·K^{-1}
L^6	Cry−I	154	63	147
L^7	Cry−I	74	96	276
$[La(L^6)(NO_3)_3]$ (**14**)	dec[b]	184		
$[Eu(L^6)(NO_3)_3]$ (**15**)	dec[b]	188		
$[Gd(L^6)(NO_3)_3]\cdot H_2O$ (**16**)	loss: 1 H_2O	150−180		
	dec[b]	187		
$[Tb(L^6)(NO_3)_3]$ (**17**)	dec[b]	198		
$[Lu(L^6)(NO_3)_3]$ (**18**)	Cry−Cry′	157	16	37
	dec[b]	177		
$[La(L^7)(NO_3)_3]$ (**19**)	dec[b]	186		
$[Eu(L^7)(NO_3)_3]$ (**20**)	Cry−Cry′	112	12	31
	dec[b]	183		
$[Lu(L^7)(NO_3)_3]\cdot H_2O$ (**21**)	Cry−Cry′	123	45	115
	loss: 1 H_2O	180−184		
	dec[b]	185		
$[La(L^6)(CF_3CO_2)_3]_2\cdot 3H_2O$ (**22**)	loss: 1.5 H_2O	150−200		
	dec[b]	213		
$[Lu(L^6)(CF_3CO_2)_3]_2$ (**23**)	dec[b]	185		

[a] Cry = crystal and I = isotropic fluid; temperature is given as the onset of the peak (Seiko DSC 220C differential scanning calorimeter, 5 °C·min^{-1}, under N_2). [b] Decomposition; see text.

Syntheses and Characterizations of the Complexes $[Ln(L^i)(NO_3)_3]\cdot xH_2O$ (i = 6, 7) and $[Ln(L^6)(CF_3CO_2)_3]_2\cdot xH_2O$. The mixing of stoichiometric quantities of L^i (i = 6, 7) with $Ln(NO_3)_3\cdot xH_2O$ (x = 2−6) or $[Ln(CF_3CO_2)_3]_n\cdot xH_2O$ (x = 1−3) in acetonitrile/dichloromethane followed by crystallization in hot acetonitrile (or heavier nitriles) gives complexes **14**−**23** in good yields (75−91%). The IR spectra are dominated by the vibrations of the ligand whose ν(C═C) and ν(C═N) stretching modes are shifted by 5−10 cm^{-1} upon complexation, as previously reported for related 1:1 complexes.[7,8] For the nitrato complexes, the two stretching bands at high energy can be easily identified (1470−1490 cm^{-1} (ν_5(N═O)); 1288−1295 cm^{-1} (ν_1-(NO_2)) and their separation (175−190 cm^{-1}) is typical of bidentate nitrate groups chelated to Ln(III).[22] For trifluoroacetate anions, the situation is less clear because $CF_3CO_2^-$ ions display low local symmetries and are known to act as monodentate, bidentate, and bridging ligands with Ln(III), thus producing intricate oligomeric or polymeric architectures.[23,24] The asymmetric stretching frequencies ν_{as}(COO) occur at 1700, 1680, and 1640 cm^{-1} for $[Ln(L^6)(CF_3CO_2)_3]_2$ (**22**, **23**), but a reliable assignment of ν_{sym}(COO) in the 1450−1500 cm^{-1} domain is prevented by the large number of vibrations exhibited by the coordinated ligand. However, the related splitting pattern observed for ν_{as}(COO) in the spectrum of $[Lu(CF_3CO_2)_3]\cdot 3H_2O$ (1740, 1670, 1620 cm^{-1}) suggests that bridging and nonbridging trifluoroacetate anions are involved in **22** and **23**, as found in the crystal structure of $[Ln(CF_3CO_2)_3(OH_2)_3]_2$.[23] To establish the molecular structures and anisometries of the complexes, crystals of $[Lu(L^6)(NO_3)_3]\cdot CH_3CN$ (**18a**) and $[Lu(L^6)(CF_3CO_2)_3]_2$ (**23**) were analyzed by X-ray diffraction.

Crystal Structure of $[Lu(L^6)(NO_3)_3]\cdot CH_3CN$ (18a). The crystal structure of **18a** shows it to be composed of a neutral complex $[Lu(L^6)(NO_3)_3]$ and an interstitial solvent molecule. L^6 adopts the expected almost planar cis-cis conformation (interplanar angles between pyridine and benzimidazole rings 8.2(3) and 11.8(3)°, Table S2, Supporting Information) resulting from its meridional tricoordination to Lu(III). The metal atom is almost contained in the plane defined by its coordinating nitrogen atoms (deviation 0.13 Å) and its coordination sphere is completed by three bidentate pseudo-C_{2v} nitrates, leading to a low-symmetry nine-coordinate site very similar to that described for $[Lu(L^8)(NO_3)_3]$. Selected bond distances and bond angles are given in Table 5, Figure 6 shows the atomic numbering scheme, and Figure 7 presents an ORTEP[13] view of the rodlike complex.

The Lu−N (2.377−2.445 Å; average 2.40 Å) and Lu−O (2.346−2.453 Å; average 2.38 Å) distances are standard, as are the N−Lu−N and O−Lu−O bite angles, which are similar to those reported for $[Lu(L^8)(NO_3)_3]$.[8] The tridentate binding unit is connected via antiperiplanar $C_{bzim}-O-CH_2-C_{phenyl}$ spacers (dihedral angles 162.1(9) and 176.9(9)°) to the lateral 4-(dodecyloxy)phenyl groups, which adopt quasi-coplanar arrangements with the benzimidazole rings to which they are connected (interplanar angles 19.9(4) and 14.7(4)°, respectively). This contrasts with the almost orthogonal arrangement of the benzimidazole and phenyl rings of one sidearm in $[Lu(L^8)(NO_3)_3]$ originating from intermolecular stacking interactions.[8] The lipophilic alkyl chain C50−C61 adopts an elongated all-trans conformation and runs approximately in the plane of the phenyl ring to which it is connected (interplanar angle 6.4(6)°). On the other hand, chain C22−C33 displays a bent orientation resulting from a specific torsion about the C22−C23 bond (dihedral angle O2−C22−C23−C24 = −60(2)°; Figure 7). Except for minor variations in the specific arrangement of peripheral substituents, we conclude that the inverted $-CH_2-O-$ and $-O-CH_2-$ spacers in $[Lu(L^8)(NO_3)_3]$ and $[Lu(L^6)(NO_3)_3]$ have negligible effects on the molecular structures of the complexes and the only significant difference is associated with the positions at which the sidearms are connected. 5-Substituted benzimidazole rings produce U-shaped arrangements of the coordinated strand as observed in $[Lu(L^8)(NO_3)_3]$,[8] while 6-substitution in $[Lu(L^6)(NO_3)_3]$ leads to I-shaped arrangements in agreement with the design of the ligands (Figure 1). To quantify the deviation from a linear arrangement of the side chains induced by the tridentate cores in complexes and free ligands, we have calculated the angles α(C10−N1−C38) for L^6 and α(C9−N1−C37) for L^5, which measure the global bending of the coordinated organic strand. In the free ligand

(22) Bünzli; J.-C. G.; Metabanzoulou, J.-P.; Froidevaux, P.; Jin, L. *Inorg. Chem.* **1990**, *29*, 3875.
(23) Junk, P. C.; Kepert, C. J.; Wei-Min, L.; Skelton, B. W.; White, A. H. *Aust. J. Chem.* **1999**, *52*, 459. Harrisson, D.; Giorgetti, A.; Bünzli, J.-C. G. *J. Chem. Soc., Dalton Trans.* **1985**, 885.
(24) Giorgetti, A.; Bünzli, J.-C. G. *Inorg. Chim. Acta* **1985**, *110*, 225 and references therein.

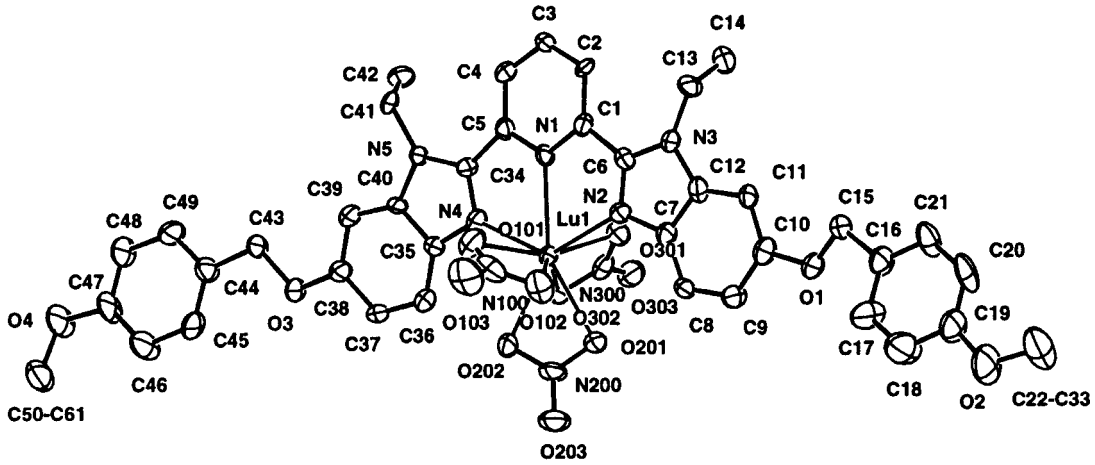

Figure 6. Atomic numbering scheme for $[Lu(L^6)(NO_3)_3]\cdot CH_3CN$ (**18a**). Ellipsoids are represented at the 40% probability level.

Table 5. Selected Bond Distances (Å) and Angles (Deg) for $[Lu(L^6)(NO_3)_3]\cdot CH_3CN$ (**18a**)

		Bond Distances			
Lu−O101	2.357(8)	Lu−O201	2.380(7)	Lu−O301	2.346(8)
Lu−O102	2.383(9)	Lu−O202	2.364(6)	Lu−O302	2.453(8)
Lu−N1	2.445(7)	Lu−N2	2.388(8)	Lu−N4	2.377(7)
N100−O101	1.28(1)	N200−O201	1.27(1)	N300−O301	1.27(1)
N100−O102	1.27(2)	N200−O202	1.28(1)	N300−O302	1.26(1)
N100−O103	1.21(2)	N200−O203	1.19(1)	N300−O303	1.23(1)
		Bite Angles			
N1−Lu−N2	65.6(3)	N1−Lu−N4	67.3(3)	N2−Lu−N4	132.8(3)
O101−Lu−O102	53.6(3)	O201−Lu−O202	54.1(2)	O301−Lu−O302	53.3(2)
		N−Lu−O Angles			
N1−Lu−O101	80.4(3)	N1−Lu−O201	152.7(2)	N1−Lu−O301	78.7(3)
N1−Lu−O102	107.4(3)	N1−Lu−O202	153.1(2)	N1−Lu−O302	112.0(2)
N2−Lu−O101	102.8(3)	N2−Lu−O201	89.9(3)	N2−Lu−O301	72.3(3)
N2−Lu−O102	73.4(3)	N2−Lu−O202	136.7(3)	N2−Lu−O302	123.5(3)
N4−Lu−O101	72.8(3)	N4−Lu−O201	134.4(3)	N4−Lu−O301	95.0(3)
N4−Lu−O102	125.7(3)	N4−Lu−O202	89.7(3)	N4−Lu−O302	71.9(2)
		O−Lu−O Angles			
O101−Lu−O201	118.6(3)	O101−Lu−O202	79.5(3)	O101−Lu−O301	158.7(3)
O101−Lu−O302	133.4(3)	O102−Lu−O201	74.6(3)	O102−Lu−O202	74.1(3)
O102−Lu−O301	138.4(3)	O102−Lu−O302	140.6(3)	O201−Lu−O301	82.5(2)
O201−Lu−O302	70.5(2)	O202−Lu−O302	70.9(2)	O202−Lu−O301	118.7(3)

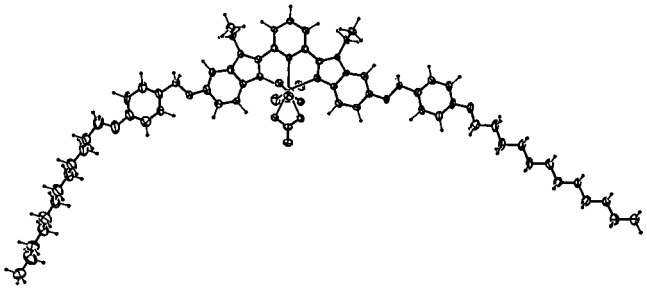

Figure 7. ORTEP[13] view of $[Lu(L^6)(NO_3)_3]$ (**18a**) perpendicular to the tridentate binding unit. Ellipsoids are represented at the 40% probability level.

L^5, bearing substituents at the 5-positions, the trans-trans conformation of the tridentate binding unit ensures a quasi-linear arrangement of the sidearms ($\alpha = 160°$), which is relaxed upon complexation (cis-cis conformation), leading to $\alpha = 109.9°$ (U-shaped arrangement) in $[Lu(L^8)(NO_3)_3]$.[8] The connection of the sidearms to the 6-positions reverses the situation, but we only obtain an intermediate value of $\alpha = 134.4°$ for the coordinated ligand in $[Lu(L^6)(NO_3)_3]$, which indicates that the trans-trans → cis-cis conformational change occurring upon complexation is accompanied by a scissoring effect of the tridentate chelating unit, bringing the benzimidazole sidearms closer and thus allowing the efficient coordination of Ln(III). A rough estimation of the molecular anisometry of $[Lu(L^6)(NO_3)_3]$, possessing idealized all-trans conformations of the alkyl chains, gives a total length of 55.8 Å (C33···C61) and a perpendicular extension of 9.2 Å (C3···O203), leading to a length:width ratio of 6.0, which can be compared to 10.0 found for free L^5. Moreover, the coordination of the $Ln(NO_3)_3$ unit in $[Lu(L^6)(NO_3)_3]$ provides a significant thickness in a direction perpendicular to the pseudoplanar tridentate core (O103···O303 = 8.0 Å) which is absent in the free ligand. No significant intra- or intermolecular stacking interactions are observed in the unit cell. The slightly bent ligands adopt wavy arrangements running along the *c* direction as a result of the head-to-tail arrangements of the alkyl chains belonging to pairs of molecules related by an inversion center; as the ligand strands deviate from linearity, the zigzag chains simultaneously progress roughly along *a* (Figure S7, Supporting Information).

Crystal Structure of $[Lu(L^6)(CF_3CO_2)_3]_2$ (23). The crystal structure of **23** is composed of centrosymmetric dimers $[Lu(L^6)(CF_3CO_2)_3]_2$ in which the metals are separated by 5.067(1) Å and connected by two bridging $CF_3CO_2^-$ anions (Figures 8 and 9, Table 6). Each Lu(III) is nine-coordinated by three heterocyclic nitrogen atoms of the tridentate aromatic unit and by six oxygen atoms arising from two monodentate (bridging)

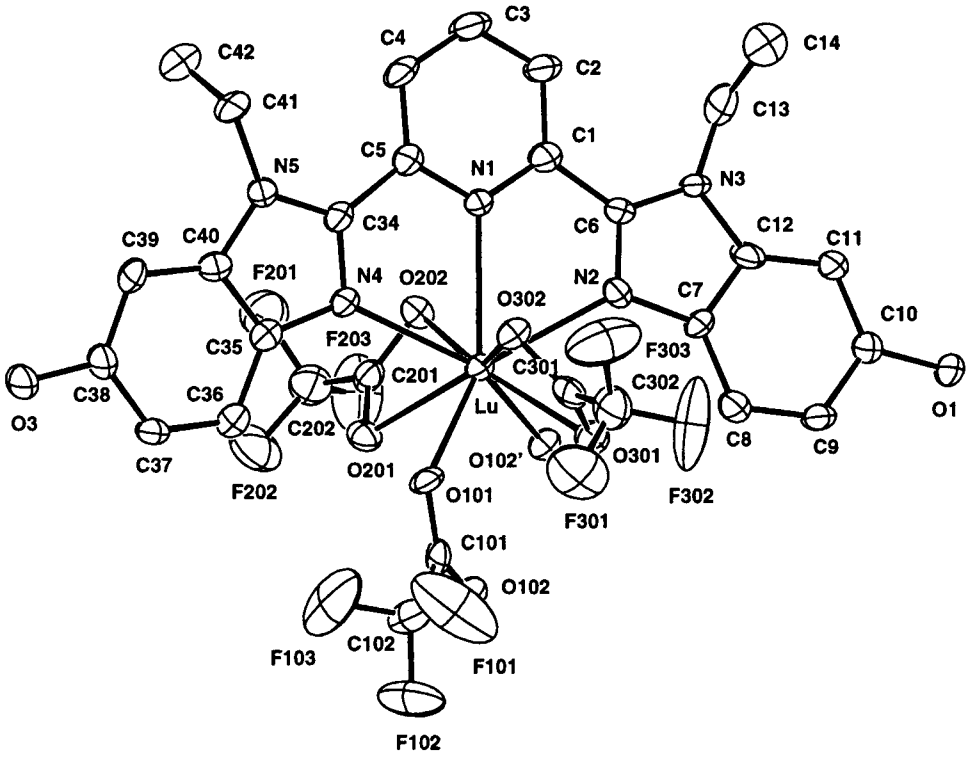

Figure 8. Atomic numbering scheme of the asymmetric unit in $[Lu(L^6)(CF_3CO_2)_3]_2$ (**23**). The numbering of the 4-(dodecyloxy)benzyl sidearms is identical to that shown in Figure 6. Ellipsoids are represented at the 40% probability level.

Table 6. Selected Bond Distances (Å) and Angles (Deg) for $[Lu(L^6)(CF_3CO_2)_3]_2$ (**23**)

		Bond Distances			
Lu−O101	2.313(6)	Lu−O201	2.428(4)	Lu−O301	2.495(6)
Lu−O102′	2.269(6)	Lu−O202	2.379(6)	Lu−O302	2.381(5)
Lu−N1	2.544(7)	Lu−N2	2.480(6)	Lu−N4	2.460(7)
C101−O101	1.24(1)	C201−O201	1.25(1)	C301−O301	1.21(1)
C101−O102	1.25(1)	C201−O202	1.24(1)	C301−O302	1.27(1)
		Bite Angles			
N1−Lu−N2	63.4(2)	N1−Lu−N4	64.9(2)	N2−Lu−N4	127.8(2)
O101−Lu−O102′	98.6(2)	O201−Lu−O202	54.9(2)	O301−Lu−O302	53.7(2)
		N−Lu−O Angles			
N1−Lu−O101	138.1(2)	N1−Lu−O201	116.3(2)	N1−Lu−O301	115.5(2)
N1−Lu−O102′	123.3(2)	N1−Lu−O202	70.2(2)	N1−Lu−O302	76.2(2)
N2−Lu−O101	138.9(2)	N2−Lu−O201	139.5(2)	N2−Lu−O301	71.4(2)
N2−Lu−O102′	74.2(2)	N2−Lu−O202	92.8(2)	N2−Lu−O302	82.3(2)
N4−Lu−O101	80.6(2)	N4−Lu−O201	72.6(2)	N4−Lu−O301	127.7(2)
N4−Lu−O102′	145.7(2)	N4−Lu−O202	76.4(2)	N4−Lu−O302	79.0(2)
		O−Lu−O Angles			
O101−Lu−O201	71.3(2)	O101−Lu−O202	125.5(2)	O101−Lu−O301	67.5(2)
O101−Lu−O302	74.4(2)	O102′-Lu-O201	74.7(2)	O102′-Lu-O202	76.5(2)
O102′-Lu-O301	81.5(2)	O102′-Lu-O302	134.2(2)	O201−Lu−O301	128.0(2)
O201−Lu−O302	138.2(2)	O202−Lu−O302	144.4(2)	O202−Lu−O301	155.8(2)

[a] Primed atom in equivalent position $1 - x$, $1 - y$, $1 - z$.

trifluoroacetate anions and two bidentate $CF_3CO_2^-$ anions, the latter being located respectively below and above the meridional plane defined by N1, N2, and N3. Lu(III) lies slightly out of this plane (deviation: 0.256 Å toward trifluoroacetate 300) and displays Lu−N distances (2.460−2.544 Å; average 2.49 Å) that are significantly longer than those observed in $[Lu(L^6)(NO_3)_3]$ (average 2.40 Å) or $[Lu(L^8)(NO_3)_3]$ (average 2.38 Å).[8] The bidentate trifluoroacetate anions are asymmetrically bound to Lu(III), displaying short (2.379−2.381 Å) and long (2.428−2.495 Å) Lu−O distances, as recently reported for the related dimetallic complex $[Lu(L^1)(OH_2)(CCl_3CO_2)_3]_2$, in which bidentate trichloroacetates exhibit a difference of 0.17 Å between the Lu−O bond distances (2.41 and 2.58 Å).[25] The Lu−O distances involving the bridging trifluoroacetates are more symmetrical and shorter (2.269−2.313 Å; average 2.29 Å), in agreement with those reported for the dimers $[Ln(CF_3CO_2)_3(OH_2)_3]_2$ (2.264−2.294 Å).[23] The ionic radius of Lu(III) calculated from Shannon's definition[26] and $r(N) = 1.46$ Å and $r(O) = 1.31$ Å is 1.057 Å, which is larger than (i) the expected value for nine-coordinate Lu(III) (1.032 Å)[26] and (ii) the radii calculated for the metal ions in $[Lu(L^6)(NO_3)_3]$ (1.028 Å) and

(25) Kepert, C. J.; Wei-Min, L.; Semenova, L. I.; Skelton, B. W.; White, A. H. *Aust. J. Chem.* **1999**, *52*, 481.
(26) Shannon, R. D. *Acta Crystallogr.* **1976**, *A32*, 751.

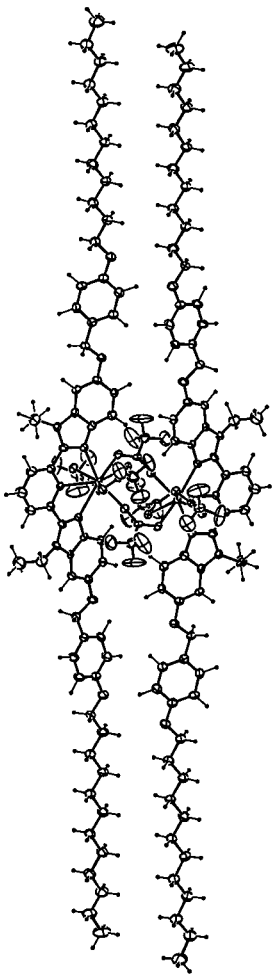

Figure 9. ORTEP[13] view of the centrosymmetric complex $[Lu(L^6)(CF_3CO_2)_3]_2$ (**23**) showing the H-shaped arrangement of the dimer. Ellipsoids are represented at the 40% probability level.

$[Lu(L^8)(NO_3)_3]$ (1.027 Å).[8] Although we do not detect strikingly short intramolecular contact distances between the parallel ligand strands, we tentatively attribute the large ionic radius and the elongated Lu−N bond distances to the bulkiness of the tridentate cores, which prevents a closer approach of the monomeric units as previously reported for $[Lu(L^1)(OH_2)(CCl_3CO_2)_3]_2$ (Lu···Lu = 5.23 Å), in which anomalously close CH···O contact distances have been observed.[25]

Each ligand strand adopts a fully elongated conformation resulting from (i) an almost planar arrangement of the five aromatic planes (interplanar angles in the range 3.1−11.3°, Table S3, Supporting Information), (ii) all-trans conformations of the dodecyloxy chains, (iii) an almost linear arrangement (deviation 4°) of the alkyl chains running in opposite directions, and (iv) a limited bending of the tridentate binding unit (α(C9−N1−C37) = 138.4°). The dimer $[Lu(L^6)(CF_3CO_2)_3]_2$ displays an H-shaped structure with a total length of 59.7 Å (C33···C33′) and a width of 15.4 Å (C3···C3′), leading to a ratio of only 3.9. The coordination of the bidentate trifluoroacetate on both sides of the meridional plane produces a considerable perpendicular thickness of 8.4 Å (C202···C302), and the core of the molecule can be described as a distorted ellipsoid. Because the centrosymmetric dimer is the unique molecular entity in the unit cell, all the molecules in the crystal are parallel and are aligned with their long axis running along the [−2,4,1] direction. Close packing of the dimers perpendicular to this direction produces weak intermolecular stacking interactions between head-to-tail pyridine−benzimidazole units, implying molecules in position *x*, *y*, *z* with that in −*x*, 1 − *y*, 1 − *z* (average interplanar distance 3.88 Å) and in *x*, *y*, *z* with 1 − *x*, −*y*, 1 − *z* (average interplanar distance 3.98 Å, Figure S8, Supporting Information).

Thermal Behavior of Complexes 14−23. All complexes **14**−**23** exhibit decomposition into a reddish liquid around 180−200 °C. No evidence for mesomorphism has been found by polarizing microscopy, and the DSC traces are dominated by a weak endotherm corresponding to the beginning of the isotropization process (Table 4), which is then masked by a considerable exothermic decomposition. Thermogravimetric analyses show the total or partial loss of solvent for complexes possessing interstitial water molecules (**16**, **21**, and **22**) prior to decomposition, while poorly reproducible losses of mass accompany the decomposition processes. The rough I-shaped arrangements of the ligand strands in $[Ln(L^6)(NO_3)_3]$ (**14**−**18**) are not sufficient to promote mesomorphism, and the thermal behavior of these complexes is similar to that observed for the U-shaped complexes $[Ln(L^3)(NO_3)_3]$;[8] we conclude that the formation of mesophases, as observed for the free ligands L^{3-5}, cannot be assigned only to the linear conformations of the strands and that polarization effects[4] and/or reduced anisometry in the complexes might prevent the formation of liquid crystalline phases. The replacement of oxidizing NO_3^- by $CF_3CO_2^-$ in **22** and **23** has no beneficial effect on the thermal properties of the complexes although their dimeric natures and H-shaped structures are significantly different from those found in $[Ln(L^6)(NO_3)_3]$. The presence of two supplementary dodecyloxy chains in $[Ln(L^7)(NO_3)_3]$ also leads to decomposition around 185 °C, but two reversible phase transitions are observed for the heavier lanthanides (Ln = Eu, Lu) when the heating process is stopped before decomposition. Careful observations by polarizing microscopy indicate that these are solid-state transitions (Cry → Cry′).

Photophysical Properties of the $[Ln(L^6)(NO_3)_3]\cdot xH_2O$ Complexes. Upon complexation of L^6 to Ln(III) ions, forming $[Ln(L^6)(NO_3)_3]$, the low energy $\pi \rightarrow \pi^*$ transitions are each split into two main components and are red-shifted by ∼2500 cm^{-1} in solution (Table 2) and in the solid state (Table 3). These electronic effects originate from the trans-trans → cis-cis conformational changes combined with the complexations to the Ln(III) ions, as previously described for $[Ln(L^3)(NO_3)_3]$[8] and theoretically supported by EHMO calculations.[16] Emissions from the lowest ligand-centered $^1\pi\pi^*$ excited states of $[Ln(L^6)(NO_3)_3]$ (Ln = La, Gd, Lu) follow the same trends and display a red shift with respect to the free ligand of 4130−5400 cm^{-1} in solution and of 3700 cm^{-1} in the solid state. In the latter case, we were not able to detect the extremely faint $^1\pi\pi^*$ emission of $[Gd(L^6)(NO_3)_3]$, which strongly overlaps with the $^3\pi\pi^*$ emission. Compared to the case of $[Lu(L^3)(NO_3)_3]$ ($^1\pi\pi^*$ at 24 510 cm^{-1}),[8] the related $^1\pi\pi^*$ state in $[Lu(L^6)(NO_3)_3]$ is significantly shifted toward lower energy (2140 cm^{-1}), in qualitative agreement with the reduced HOMO−LUMO gap predicted for the free ligand when π-donor oxygen atoms are bound to the 6-positions of the benzimidazole sidearms. It is thus not surprising that ligand-centered $^3\pi\pi^*$ excited states in $[Ln(L^6)(NO_3)_3]$ (0−0 phonon transitions: 19 610, 19 230, and 19 230 cm^{-1} for Ln = La, Gd, and Lu, respectively; solid state, 77 K) are red-shifted compared to those found in $[Ln(L^3)(NO_3)_3]$ (0−0 phonon transitions: 21 800 and 20 920 cm^{-1} for Ln = Gd, Lu, respectively; solid state, 77 K).[8] In $[Eu(L^6)(NO_3)_3]$ (**15**), an efficient $L^6 \rightarrow$ Eu(III) energy transfer quenches the ligand-centered emission, providing a faint Eu-centered luminescence at room temperature. Decreasing the temperature restores an

Table 7. Corrected Integrated Intensities (I_{rel}) and Main Identified Eu ^7F_j Energy Levels (cm^{-1}; $J = 1-4$; Origin $^7F_0$) for $[Eu(L^6)(NO_3)_3]$ (**15**) As Calculated from Luminescence Spectra in the Solid State at 10 K

level	site I[a]	I_{rel}	site II[b]	I_{rel}
$^7F_0$ (ν_{exc})[c]	17239		17211	
$^7F_1$	287	1.00	330	1.00
	391		369	
	448		400	
$^7F_2$	960	4.02	950	7.43
	1020		983	
	1036		1010	
	1056		1069	
	1131		1146	
$^7F_3$	1834	0.08	1862	0.09
	1874		1881	
	1884		1939	
	1923			
$^7F_4$	2541	0.89	2572	1.04
	2592		2599	
	2620		2636	
	2650		2711	
	2688		2848	
	2963			

[a] Nonhydrated crystals. [b] Hydrated crystals. [c] Energy of the $^5D_0 \leftarrow {}^7F_0$ transition (given in cm^{-1}) used as λ_{exc} for the laser-excited emission spectra.

intense red emission, pointing to a thermally activated energy back-transfer occurring between the $^3\pi\pi^*$ and Eu($^5D_0$) states, which are separated by only 1980 cm^{-1} (taking the 0−0 phonon transition into account) compared to 4550 cm^{-1} in $[Eu(L^3)(NO_3)_3]$.[8] Excitation via the ligand-centered $^1\pi\pi^*$ states or direct laser excitation of the $^5D_0 \leftarrow {}^7F_0$ transition of nonhydrated microcrystals of $[Eu(L^6)(NO_3)_3]$ at 10 K produce very similar emission spectra which are each dominated by an intense $^5D_0 \rightarrow {}^7F_2$ transition (Table 7). The maximum multiplicities ($2J + 1$) observed for $^5D_0 \rightarrow {}^7F_j$ ($j = 1, 2$; Table 7) together with the sizable relative intensity of the $^5D_0 \rightarrow {}^7F_2$ transition point to an Eu(III) ion in a low-symmetry site, which is compatible with the C_1 symmetry observed in the crystal structure of the model complex $[Lu(L^6)(NO_3)_3]\cdot CH_3CN$ (**18a**). The unique transition observed in the $^5D_0 \leftarrow {}^7F_0$ excitation profile indicates a single crystalline site (site I), and its energy of 17 239 cm^{-1} at 10 K (17 251 cm^{-1} at 295 K; correction 1 cm^{-1}/24 K)[27] is close to that predicted by the empirical equation of Frey and Horrocks[28] (17 248 cm^{-1} at 295 K) for Eu(III) coordinated by six oxygen atoms of nitrate anions ($\delta_O(NO_3^-) = -13.3$)[7] and three heterocyclic nitrogen atoms (δ_N(N-heterocycle) = −15.3).[29] The Eu($^5D_0$) lifetime at 10 K is 1.56(1) ms for $[Eu(L^6)(NO_3)_3]$, which confirms the absence of OH oscillators directly bound to Eu(III), and it can be compared to those found for $[Eu(L^2)(NO_3)_3]$ (R^1 = octyl) (1.15 ms at 4 K),[7] $[Eu(L^2)(NO_3)_3(MeOH)]$ (R^1 = methyl) (0.86 ms at 4 K),[7] and $[Eu(L^3)(NO_3)_3(OH_2)]$ (0.60 ms at 10 K),[8] in which respectively zero, one, and two OH oscillators are bound to Eu(III). The observed decrease in the Eu $^5D_0$ lifetime with increasing temperature (1.56(1) ms at 10 K, 0.12(1) ms at 275 K; Table S4, Supporting Information) in $[Eu(L^6)(NO_3)_3]$ is typical for the existence of a $^5D_0 \rightarrow {}^3\pi\pi^*$ energy back-transfer associated with the small energy gap between these levels. When the microcrystals are separated from the mother liquor and filtered off, the $^5D_0 \leftarrow {}^7F_0$ excitation profile features a second peak at slightly lower energy (site II: 17 211 cm^{-1} at 10 K, 17 225 cm^{-1} at 295 K; Figure 10) with a shorter lifetime (1.14(1) ms at 10 K). The selective excitation of this site produces an emission spectrum with a slightly different crystal field splitting (Table 7), but the temperature dependence of the Eu $^5D_0$ lifetime parallels that found for site I, in agreement with a minor modification of the Eu(III) coordination sphere between sites I and II. As previously demonstrated for dimetallic lanthanide helicates,[30] the effect of interstitial water molecules in the second sphere may alter the symmetry, the nephelauxetic parameters, and the lifetime of the Eu(III) site, and we suspect that similar effects are responsible for the appearance of site II. The reduction of $\tau(Eu(^5D_0))$ from 1.56 to 1.14 ms between sites I and II corresponds to a quenching contribution of $\Delta k = 0.24$ ms^{-1}, a value very close to that found for the nine-coordinate complex $[Eu(oda)_3\cdot H_2O]$ (oda is oxydiacetate; $\Delta k = 0.26$ ms^{-1}),[31] in which the second-sphere water molecule resides 5.05 Å from Eu(III), and it also matches the average correction of $\Delta k = 0.25$ ms^{-1} proposed by Parker and co-workers[32] for unbound water molecules. We thus tentatively assign site II to a nine-coordinate Eu(III) site slightly distorted by the presence of water molecules in the second sphere and interacting with ligands by hydrogen bonds and/or electrostatic forces.

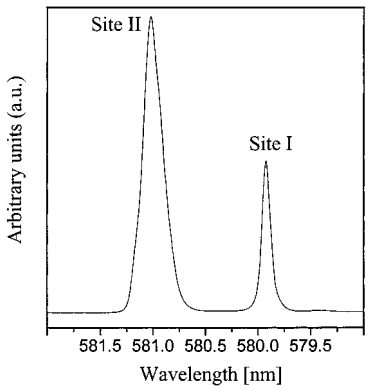

Figure 10. $^7F_0 \rightarrow {}^5D_0$ excitation profile for hydrated $[Eu(L^6)(NO_3)_3]$ showing sites I and II (λ_{an}: $^5D_0 \rightarrow {}^7F_2$).

Structures of the $[Ln(L^6)(NO_3)_3]\cdot xH_2O$ Complexes in Solution. The ^1H NMR spectra of $[Ln(L^6)(NO_3)_3]$ (Ln = La, Eu, Lu) in $CDCl_3$ and CD_3CN closely match those previously described for $[Ln(L^3)(NO_3)_3]$ under the same conditions and imply identical behaviors in solution.[8] In each case, we observe a single neutral species in $CDCl_3$ assigned to $[Ln(L^6)(NO_3)_3]$, while a partial decomplexation of the nitrate group according to eq 1 occurs in CD_3CN, thus leading to two complexes in

$$[Ln(L^6)(NO_3)_3] + nCH_3CN \rightleftharpoons [Ln(L^6)(NO_3)_2(CH_3CN)_n]^+ + NO_3^- \quad (1)$$

thermodynamic equilibrium. In all cases, the observation of NOE effects between $H^{8,9}$ and H^2 indicates that the ligand strand adopts a cis-cis conformation associated with its tricoordination to Ln(III). At first sight, the ^1H NMR spectrum of $[Lu(L^6)(CF_3CO_2)_3]_2$ (**23**) in $CDCl_3$ appears very similar to that observed

(27) Bünzli, J.-C. G. In *Lanthanide Probes in Life, Chemical and Earth Sciences*; Bünzli, J.-C. G., Choppin, G. R., Eds.; Elsevier Publishing Co.: Amsterdam, 1989; Chapter 7.
(28) Frey, S. T.; Horrocks, W. D., Jr. *Inorg. Chim. Acta* **1995**, *229*, 383.
(29) Piguet, C.; Rivara-Minten, E.; Hopfgartner, G.; Bünzli, J.-C. G. *Helv. Chim. Acta* **1995**, *78*, 1541. Piguet, C.; Bünzli, J.-C. G.; Bernardinelli, G.; Hopfgartner, G.; Petoud, S.; Schaad, O. *J. Am. Chem. Soc.* **1996**, *118*, 6681.
(30) Piguet, C.; Bünzli, J.-C. G.; Bernardinelli, G.; Hopfgartner, G.; Williams, A. F. *J. Am. Chem. Soc.* **1993**, *115*, 8197.
(31) May, P. S.; Richardson, F. S. *Chem. Phys. Lett.* **1991**, *179*, 277.
(32) Beeby, A.; Clarkson, I. M.; Dickins, R. S.; Faulkner, S.; Parker, D.; Royle, L.; de Sousa, A. S.; Williams, J. A. G.; Woods, M. *J. Chem. Soc., Perkin Trans. 2* **1999**, 493.

Table 8. Proton NMR Shifts (vs TMS) for the Main Complex of $[Lu(L^6)(CF_3CO_2)_3]_2$ (**23**) in $CDCl_3$ at Various Temperatures[a]

	δ							
T, K	H^1	H^2	H^3	H^4	H^5	H^9	% maj[b]	% min[c]
233	8.23	7.74	8.31	7.08	6.88	4.84	70	30
253	8.22	7.76	8.33	7.09	6.88	4.88	80	20
294	8.22	7.83	8.37	7.13	6.89	4.98	86	16
323	8.21	7.85	8.38	7.14	6.89	5.00	100	0

[a] See Chart 1 for numbering scheme. [b] Quantity of major species. [c] Quantity of minor species.

for $[Lu(L^6)(NO_3)_3]$ in CD_3CN and implies the existence of two different complexes of average C_{2v} symmetries in slow dynamic exchange on the NMR time scale at room temperature (Table 8). The major species (86%) displays $^1H-^1H$ COSY and NOESY spectra compatible with a planar arrangement of the meridionally tricoordinated tridentate unit similar to that found in $[Lu(L^6)(NO_3)_3]$. Variable-temperature NMR spectra show that the concentration ratio of the two complexes varies from 70:30 at 233 K to 100:0 at 323 K, pointing to complexes in thermodynamic equilibrium (Table 8). Interestingly, the ^{19}F NMR spectrum at 298 K displays a single peak (87.1 ppm vs C_6F_6), which implies that all trifluoroacetate anions rapidly exchange on the NMR time scale. Low-temperature measurements (223 K) do not show any splitting of this signal, and the addition of an excess of trifluoroacetate (introduced as the salt $^nBu_4NCF_3CO_2$) does not produce a new signal, but a slightly broadened peak is observed at 88.9 ppm, close to the position of the peak for free $CF_3CO_2^-$ (89.9 ppm). We thus conclude that the $CF_3CO_2^-$ ions are labile for $[Lu(L^6)(CF_3CO_2)_3]_2$ in solution, leading to fast intra- and intermolecular exchange processes on the NMR time scale, which are difficult to correlate with the dimer found in the crystal structure of **23**. To further investigate the structure of the main species in solution, we prepared in situ the analogous paramagnetic complex $[Yb(L^6)(CF_3CO_2)_3]_x$ by mixing L^6 with $Yb(CF_3CO_2)_3$. As expected,[29] the ^1H NMR spectrum is spread over 50 ppm ($-10 \rightarrow +40$ ppm) and reflects essentially a single species with at least an average C_{2v} symmetry which is compatible with monomeric ($x = 1$, average idealized symmetry C_{2v}) or dimeric ($x = 2$, average idealized symmetry D_{2h}) complexes. Minor species (<10%) are difficult to detect as a result of the broadening of the signal due to the coupling of nuclear and electronic magnetic moments. No attempt was made to strictly assign the observed signals to the different protons, and we consider this spectrum as the fingerprint of the Yb complex in solution. Upon mixing stoichiometric quantities of $[Lu(L^6)(CF_3CO_2)_3]_x$ and $[Yb(L^6)(CF_3CO_2)_3]_x$, we observed an ^1H NMR spectrum corresponding exactly to the addition of the spectra of the pure complexes and no signal corresponding to the hypothetical mixed dimer $[YbLu(L^6)(CF_3CO_2)_3]_2$ was detected even after 10 days. These observations combined with the ^{19}F NMR spectrum of the latter mixture, which displays a single average signal at 86.7 ppm, lead to the conclusion that the dimeric complexes evidenced in the solid state are mainly dissociated in solution to give monomeric $[Ln(L^6)(CF_3CO_2)_3]$ complexes in which the trifluoroacetate anions undergo fast intra- and intermolecular exchange processes. We tentatively assign the minor signals observed for Ln = Lu at room temperature to traces of the dimer in thermodynamic equilibrium with the major monomeric complex.

Conclusion

Our structural investigations of 5- and 6-substituted bis(benzimidazol-2-yl)pyridine units in L^{3-7} fully support the interconversions between I- and U-shaped arrangements of the ligand strands summarized in Figure 1. For the free ligands, the trans-trans conformations of the tridentate binding units provide rodlike molecules only when the semilipophilic sidearms are connected to the 5-positions (L^{3-5}), and these edifices are compatible with the formation of calamitic mesophases at moderate temperatures. Any mesomorphism is removed for U-shaped 6-substituted ligands ($L^{6,7}$). On the other hand, complexation to Ln(III) ions forces the tridentate units to adopt a cis-cis conformation compatible with linear arrangements of the side chains only for 6-substituted receptors as in $[Ln(L^6)(NO_3)_3]$. However, complexation of the tridentate binding unit is also associated with a scissoring effect, which brings the benzimidazole sidearms closer and induces a deviation from linearity. The main consequence is a more pronounced bending of the complexed ligand strand in $[Ln(L^6)(NO_3)_3]$ compared to the I-shaped arrangement found in the related free ligand L^5, which reduces the axial anisometry. At first sight, this could partially explain our failure to induce mesomorphism in 1:1 $[Ln(L^6)(NO_3)_3]$ complexes, but the large perpendicular extensions produced by the complexation of bulky $Ln(NO_3)_3$ entities together with polarization effects may also contribute to the removal of liquid crystalline properties. The positions and natures of the semilipophilic sidearms in L^{3-7} also affect the ligand-centered electronic properties, which is a crucial point if applications as luminescent relays in LCD devices are foreseen.[33] For synthetic reasons, oxygen linkers were connected directly to the benzimidazole rings in L^{5-6}, but detailed photophysical studies show that the resulting low-energy $^1\pi\pi^*$ and $^3\pi\pi^*$ excited states have deleterious effects on the sensitization of Eu(III) in $[Eu(L^6)(NO_3)_3]$, whose luminescence is essentially quenched at room temperature. Our theoretical approach using the semiempirical ZINDO method suggests that this effect is inherent to the connection of π-donor atoms (such as oxygen atoms) to the benzimidazole rings and that further design of rodlike receptors based on this tridentate binding unit should consider the use of methylene (analogous of L^3) or carboxylate (analogous of L^4) connectors. Finally, the replacement of nitrate counteranions by trifluoroacetates has no beneficial effects on the mesomorphism, but the tendency of carboxylates to bridge Ln(III) ions produces H-shaped centrosymmetric dimers in the solid state which are attractive platforms for both calamitic and discotic metallomesogens.[34]

Acknowledgment. We gratefully acknowledge Ms. H. Lartigue, Ms. V. Foiret, and Mr. X. Melich for excellent technical assistance. J.-C.G.B. thanks the Fondation Herbette (Lausanne) for the gift of spectroscopic equipment. This work was supported by grants from the Swiss National Science Foundation.

Supporting Information Available: Listings of elemental analyses for complexes **14**−**23**, selected least-squares-plane data for $[Lu(L^6)(NO_3)_3]\cdot CH_3CN$ (**18a**) and $[Lu(L^6)(CF_3CO_2)_3]_2$ (**23**), and lifetimes of the $Eu(^5D_0)$ level in $[Eu(L^6)(NO_3)_3]$ (**15**) at various temperatures (Tables S1−S4), energy-level and frontier orbital diagrams calculated with ZINDO[18] for L^{8-10} (Figures S1−S6), views of the packings in the unit cells of **18a** and **23** (Figures S7 and S8), and X-ray crystallographic files, in CIF format, for **18a** and **23**. This material is available free of charge via the Internet at http://pubs.acs.org.

IC000338U

(33) Weder, C.; Sarwa, C.; Montali, A.; Bastiaansen, C.; Smith, P. *Science* **1998**, *279*, 835.
(34) Ghedini, M.; Pucci, D.; Crispini, A.; Aiello, I.; Barigelletti, F.; Gessi, A.; Francescangeli, O. *Appl. Organomet. Chem.* **1999**, *13*, 565. Ghedini, M.; Crispini, A. *Comments Inorg. Chem.* **1999**, *21*, 53.